Observational activation of anterior cingulate cortical neurons coordinates hippocampal replay in social learning

Authors: Xiang Mou[1]*, Daoyun Ji[1,2,3]*

Affiliations:
[1]Department of Neuroscience, [2]Department of Molecular and Cellular Biology, Baylor College of Medicine; One Baylor Plaza, Houston, TX 77030, USA.
[3]Lead Contact

*Correspondence: xmou@bcm.edu (X.M.); dji@bcm.edu (D.J.)

Abstract: Social learning enables a subject to make decisions by observing the actions of another. How neural circuits acquire relevant information during observation to guide subsequent behavior is unknown. Utilizing an observational spatial working memory task, we show that neurons in the rat anterior cingulate cortex (ACC) associated with spatial trajectories during self-running in a maze are activated when observing another rat running the same maze. The observation-induced ACC activities are reduced in error trials and are correlated with activities of hippocampal place cells representing the same trajectories. The ACC activities during observation also predict subsequent hippocampal place cell activities during sharp-wave ripples and spatial contents of hippocampal replay prior to self-running. The results support that ACC neurons involved in decisions during self-running are reactivated during observation and coordinate hippocampal replay to guide subsequent spatial navigation.

Keywords: Observational learning, spatial navigation, anterior cingulate cortex, hippocampus, place cells, replay

INTRODUCTION

Observational learning, a means of social learning, takes the form of watching and/or imitating the behavior of others to learn (Bandura, 1997). This type of learning is widespread in a range of species including humans and rodents (Heyes, 1996; Meltzoff et al., 2009). Unlike learning through self-action, observational learning often involves observers making decisions contingent upon others' actions. Although recent studies have begun to reveal the neural activities associated with observational learning (Allsop et al., 2018; Danjo et al., 2018; Jeon et al., 2010; Leggio et al., 2000; Mou and Ji, 2016; Olsson and Phelps, 2007; Omer et al., 2018), it remains unknown how neural circuits process specific information acquired during observation to guide subsequent behavior.

The anterior cingulate cortex (ACC), a brain area involved in decision making (Kane et al., 2022), also plays a key role in observational learning (Burgos-Robles et al., 2019). On one hand, previous studies show that ACC neurons are modulated by emotional attributes important for decision making, such as reward or shocks associated with stimuli or places (Johansen et al., 2001; Mashhoori et al., 2018). Strong evidence also exists that activities of ACC neurons encode the valence or value of stimuli to be used for decision making or as a result of decision making (Caracheo et al., 2018; Hillman and Bilkey, 2010; Monosov, 2017). On the other hand, ACC can be activated when observing another subject in pain or receiving a reward (Carrillo et al., 2019; Schneider et al., 2020). ACC is also required for an observer to acquire fear responses to a context or stimulus after observing another subject doing so (Jeon et al., 2010; Olsson and Phelps, 2007), and ACC neurons are activated during fear acquisition through observation (Allsop et al., 2018).

These known functions of ACC raise an important question: How are specific ACC neuronal activities occurring during observation involved in the observer's subsequent decisions? To gain insights into this question, we set out to study ACC neurons in rats performing an observational spatial working memory task (oSWM) (Mou et al., 2022), during which an observer rat (OB), after observing the run of a demonstrator (Demo) in the maze, decides which spatial trajectories in a T-maze to run for water reward, from a nearby, separate observation box.

Since places and spatial trajectories are encoded by hippocampal place cells (O'Keefe and Dostrovsky, 1971; Wilson and McNaughton, 1993), it is not surprising that the oSWM task depends on the CA1 area of the hippocampus (Mou et al., 2022). It is known that, as an animal travels through a spatial trajectory, hippocampal place cells are activated sequentially (Harris et al., 2003). The sequential activation can be replayed during awake resting or reward consumption (Diba and Buzsaki, 2007; Foster and Wilson, 2006), together with the concurrent high-frequency sharp-wave ripples (SWRs) in the CA1 local field potentials (LFPs) (Buzsaki et al., 1992; Csicsvari et al., 2000). Evidence exists that such awake replay may be a neural substrate underlying memory recall or planning for future spatial trajectories (Carr et al., 2011; Jadhav et al., 2012; Pfeiffer and Foster, 2013; Wu et al., 2017). Indeed, in the oSWM task, awake replay of CA1 place cell activities associated with self-running in the T-maze occurs remotely in the observation box and this remote awake replay predicts subsequent self-running trajectories in the maze (Mou et al., 2022), consistent with a role of awake replay in spatial planning.

In this study, we examine ACC neurons in the oSWM task and their interactions with CA1 place cells, aiming to understand how ACC activities during observation are related to the hippocampal replay that presumably plans for future spatial trajectories. We focus on the hypothesis that ACC neurons acquire the information key to spatial decisions during observation and use it to coordinate the replay of CA1 place cells for planning subsequent spatial trajectories during self-running.

RESULTS

The data analyzed in this study were obtained from 16 rats, each as a well-trained OB performing the oSWM task. Briefly, in each trial of the task, an OB stayed in an observation box while a Demo ran along a nearby T-maze and made a random choice of a left or right (outbound) trajectory for water (**Figure 1A**). The OB was rewarded with water in the box if the animal poked on the same side of the box as the Demo's in the maze within 10 s. After the Demo returned along a left or right (inbound) trajectory and was then confined in a rest box, the OB was transported to the central arm of the T-maze. The OB was rewarded with water if the animal chose the same outbound trajectory as the Demo's. The OB then returned along the same inbound trajectory in the maze as the Demo's, before being moved back to the observation box for the next trial. Each daily session consisted of ~40 trials. After training, all OBs learned to synchronize their pokes in the box with their Demo's pokes in the maze and followed their Demo's trajectories during subsequent self-running in ~85% of the trials (Mou et al., 2022).

ACC-dependence of the oSWM task

Before analyzing ACC neurons, we first asked whether the OBs' performance required an intact ACC. We infused N-methyl-D-aspartate (NMDA) into the ACC to induce lesions in a group of OBs (N = 5) and compared their performance to another group (N = 5) with vehicle infusion (**Figure 1B**) in 3 sessions tested 2 weeks after (After) and in 3 sessions before (Before) the infusion.

We computed a poke performance curve for each session to measure the synchronization of pokes between an OB in the box and the corresponding Demo in the maze (see Methods) (Mou et al., 2022). The average poke performance curve of the vehicle group in After peaked close to time 0, whereas that of the NMDA group displayed a delayed, weak peak (**Figure 1C**). The curves were significantly different between the two groups in After (*Two-way ANOVA*: $F_{(1,329)} = 19$, $P = 1.7 \times 10^{-5}$), but not in Before ($F_{(1,329)} = 3.6$, $P = 0.060$). This difference was mainly due to the decreased performance in the NMDA group after infusion (Before vs. After, *Two-way ANOVA*: $F_{(1,329)} = 6.4$, $P = 0.012$). Therefore, the performance of the NMDA group in the box was impaired by the ACC lesion.

In the maze, the performance of the NMDA group, measured by the percentage of correct trials, was also significantly lower than that of the vehicle group in After (NMDA: 53.3 ± 2.0%, mean ± SEM, N = 15 sessions from 5 rats; Vehicle: 80.6 ± 1.6%, N = 15; $F_{(1,29)} = 134$, $P = 9.2 \times 10^{-12}$), but not in Before (NMDA: 84.1 ± 1.9%, N = 15; Vehicle: 83.6 ± 1.1%, N = 15; $F_{(1,29)} = 2.7$, $P = 0.11$; **Figure 1D**). The difference in After was not due to a locomotion deficit, because there was no significant difference in the mean duration of running laps between the two groups in After (NMDA: 64.1 ± 1.7 s, Vehicle: 62.9 ± 1.7 s, $P = 0.60$, two-sided t-test). The data indicate that the ACC lesion impaired the maze

performance of the NMDA group. Therefore, besides the CA1 area of the hippocampus (Mou et al., 2022), the oSWM task also depends on ACC.

Activation of ACC selective cells during observation

We next analyzed ACC cells in the oSWM task, which were recorded simultaneously with CA1 place cells from 6 well-trained OBs. In total, 492 ACC cells were obtained from 5 OBs in 19 sessions with a well-trained Demo as described above, referred to as the standard Demo condition. In addition, we also recorded ACC cells in two control conditions (see Methods): 248 ACC cells from 3 OBs in 11 sessions with the Demo replaced by a moving object (Object) and 309 ACC cells from 5 OBs in 13 sessions with the Demo removed (Empty).

We first defined left and right trials of a session by the Demo's choice of the left and right side of the maze, respectively. Since the OBs were well-trained, they also ran the same left (or right) trajectories correctly in the maze in the majority of the left (or right) trials, after getting rewarded in the left (or right) side of the box (although a well-trained OB sometimes poked on the wrong side of the box first, the rat quickly switched to the other side and got rewarded in the box in almost all the left/right trials).

We noticed that many ACC cells distinguished the left from the right side of the maze during self-running. We call such cells ACC selective cells. For example, an ACC left-selective cell fired with higher rates on the left inbound trajectory in left trials than on the corresponding trajectory in right trials, and an ACC right-selective cell had higher rates on a segment of the right outbound trajectory in right trials than on the corresponding segment in left trials (**Figure 2A**). Because previous studies showed that ACC cells encode valence, value, or decision associated with a stimulus or location (Caracheo et al., 2018; Hillman and Bilkey, 2010; Kane et al., 2022; Mashhoori et al., 2018; Monosov, 2017), we reasoned that the activities of such ACC selective cells likely reflected the decision or reward associated with the chosen trajectory or segment during self-running. Since our goal was to investigate the function of ACC cells in observational learning, not the exact attributes of a trajectory/segment to be encoded during self-running, we focused on whether and how these ACC cells reflecting the left or right choice in the maze were also activated during observation in the box.

To quantitatively identify ACC selective cells, we computed the firing rate of each ACC cell during each running lap on the left or right side of the maze (inbound and outbound trajectories combined, without identifying specific active segments). We assigned a selectivity index (SI) to quantify the difference in the mean rate between left and right laps (see Methods), which ranged between -1 (most left-selective) to 1 (most right-selective). An ACC cell was classified as selective if the difference was statistically significant. Indeed, the two example cells above were classified as such cells (Left-selective cell: $P = 3.2 \times 10^{-3}$, two-sided *t*-test; Right-selective cell: $P = 2.6 \times 10^{-11}$; **Figure 2C**). A total of 202 ACC cells (41%) were selective during self-running in the T-maze under the Demo condition (under Demo). Only ACC selective cells were included in the rest of the analysis on ACC neural activities, unless specified otherwise.

We examined firing activities of these ACC cells in the box in each trial, particularly during a delay window between the time when a Demo crossed the choice point in the maze and

when the corresponding OB made the first correct (rewarded) poke in the box (**Figure S1A**). We focused on this delay window because it was the time for the OB to observe the Demo's choice. The distribution of this window's duration across all trials of all OBs under Demo had a dominant peak at ~2 s (**Figure S1B**). In order to examine ACC cells within a time period with relatively consistent behavior across all trials (animals in occasional long delay windows typically checked other parts of the box or did not pay attention before poking), we defined a delay period for each trial as the 2 s period before the OB's first correct poke in the box. The head position and head direction of a typical OB within this 2-s delay period for all left and right trials of a session displayed consistent left and right swings as expected (**Figure S1C-D**).

We found that many ACC cells fired differently during delay periods in the box between left and right trials. For example, the ACC cells selective to the left or right side of the maze (**Figure 2A**) also had higher firing rates during delay periods of left or right trials in the box (**Figure 2B**), meaning that they were also left- and right-selective in the box with significant SIs (Left-selective cell: $P = 4.6 \times 10^{-7}$, two-sided *t*-test; Right-selective cell: $P = 1.3 \times 10^{-4}$; **Figure 2C**).

We computed the SI in the maze and in the box for each ACC selective cell under Demo and found that the maze and box SIs were significantly correlated ($R = 0.25$, $P = 1.4 \times 10^{-4}$, *Pearson's r*; **Figure 2D**). We counted the number of ACC cells with significant SIs on the same side of the box and the maze (same-side selectivity) and compared to the chance-level distribution, obtained by randomly shuffling each cell's rates during delay periods among left and right trials (see Methods). We found that 34% of ACC selective cells had same-side selectivity, which was significantly higher than the chance level ($Z = 4.1$, $P = 2.1 \times 10^{-5}$, *Z*-test**, Figure 2E**).

We performed the same analysis on ACC cells recorded in sessions under the two control (Object, Empty) conditions. The number of correct trials was close to chance level (50%) under both Object and Empty conditions, which still allowed for the identification of ACC selective cells. The percentage of ACC selective cells (among all recorded ACC cells) identified under these conditions was comparable to that under Demo (**Figure S2A**). However, their SIs in the maze were not correlated with those in the box (Object: $R = -0.19$, $P = 0.97$; Empty: $R = -0.0019$, $P = 0.51$, *Pearson's r*; **Figure 2D**). In addition, the number of ACC cells with same-side selectivity was not significantly different from the chance level under either Object (24%, $Z = -0.47$, $P = 0.68$, *Z*-test) or Empty (28%, $Z = 1.1$, $P = 0.14$; **Figure 2E**).

As a control, we also analyzed the ACC cells with opposite-side selectivity in the box. We found that the number of these ACC cells was significantly less than the chance level under Demo, and not significantly different from the chance level under Object or Empty (**Figure S2B-C**).

Taken together, our data show that ACC cells selective to the left/right side of the maze were also selective to the same side in the box during delay periods under Demo condition. The presence of same-side selectivity of ACC cells, in contrast to opposite-side selectivity, indicates that the ACC cells selective to the observed trajectories in the maze were preferentially activated during observation in the box, prior to self-running on the

same trajectories. The lack of same-side selectivity of ACC cells under Object or Empty conditions suggests that this activation was not simply due to the movement of OBs to the same side in the box. Therefore, our data support that observation activates those ACC cells specifically associated with the observed, and thus the subsequent future, trajectories.

Reduced ACC activation during observation in error trials

To provide further evidence for the involvement of ACC activation in subsequent self-running, we asked whether the activation during observation was compromised in error trials. An error trial was defined as one in which an OB ran to the side in the maze opposite to the Demo's choice, even after receiving water in the box on the same side (**Figure 3A-B**). Since the OBs in this study were well-trained, error trials were rare under Demo (11% ± 2% per session). Nevertheless, we examined ACC cells in those sessions that contained at least 3 error trials.

For an ACC cell with same-side selectivity, we compared its activities during delay periods between correct and error (≥3) trials on its preferred side of the box (left for ACC left-selective cells, right for ACC right-selective cells). ACC cells typically displayed higher rates in correct trials than in error trials under Demo, which was quantified by a positive rate difference index (DI; **Figure 3A-B**). For those ACC cells with same-side selectivity, their mean DI was significantly different from 0 under Demo (0.13 ± 0.04, N = 52, P = 0.0016, two-sided t-test), but not under Object (-0.03 ± 0.02, N = 82, P = 0.20) or Empty (0.01 ± 0.02, N = 127, P = 0.51; **Figure 3C**). The mean DI under Demo was also significantly higher than those under Object and Empty ($F_{(1,257)}$ = 9.3, $P = 1.2 \times 10^{-4}$, *One-Way ANOVA*). In addition, the fraction of ACC cells with same-side selectivity that displayed a significant positive DI was greater than the chance level, obtained by randomizing rates among correct and error trials, under Demo (14%, Z = 3.5, $P = 2.1 \times 10^{-4}$, Z-test), but not under Object (3.8%, Z = -0.62, P = 0.73) or Empty (3.9%, Z = -0.46, P = 0.68; **Figure 3D**). For ACC cells with same-side selectivity, their mean DI during delay periods on their non-preferred side (left for ACC right-selective cells, right for ACC left-selective cells), was not significantly different from 0 and the fraction of cells with a significant positive DI was no more than the chance level under Demo, Object or Empty (**Figure S3**).

Our data thus show that the activation of ACC cells with same-side selectivity during observation was reduced when OBs made errors during self-running in the maze, consistent with a role of observation-activated ACC activities in subsequent spatial decisions.

Interaction between ACC cells and CA1 place cells during observation

Since spatial trajectories in the maze are encoded by hippocampal place cells (Harris et al., 2003; O'Keefe and Dostrovsky, 1971; Wilson and McNaughton, 1993), we next asked whether ACC cells selective to a trajectory in the maze interacted with those CA1 place cells encoding the same trajectory during delay periods in the box.

We identified the CA1 place cells active during self-running in the maze. A total of 762, 499, and 621 CA1 place cells were identified under Demo, Object, and Empty,

respectively. We checked whether CA1 place cells selectively active on left/right trajectories in the maze displayed similar selectivity during delay periods in the box and found no significant same-side or opposite-side selectivity under either Demo, Object, or Empty (**Figure S4**). Since CA1 cells often had relatively low mean rates (<2 Hz) during delay periods (**Figure S4A**), we examined CA1 place cells at the population level by combining those selective to the left or right trajectories of the maze (inbound and outbound combined) in each session into a left or right CA1 ensemble (see Methods). We then asked how ACC cells selective to the left/right side of the maze interacted with the CA1 ensembles selective to the same or opposite side (same- or opposite-side ensembles) during delay periods in the box (**Figure 4A**).

For this purpose, we computed a cross-correlation curve between the firing rates of an ACC cell and those of a CA1 ensemble (all spikes of all cells in an ensemble combined) within 200-ms time bins of delay periods. As shown in **Figure 4B**, an example ACC cell displayed a cross-correlation curve with a peak around the time lag 0 with its same-side CA1 ensemble, but not with its opposite-side one. We thus used the correlation value at the time lag 0 to quantify the interaction between an ACC cell and a CA1 ensemble.

During delay periods in the observation box under Demo (**Figure 4C**), ACC cells on average had a significant mean correlation with their CA1 same-side ensembles (same-side correlation: 0.044 ± 0.014, N = 202, P = 0.0028, two-sided t-test compared to 0), but not with their opposite-side ones (opposite-side correlation: 0.0056 ± 0.011, N = 202, P = 0.60). In contrast, there was no significant same- or opposite-side correlation under either Object (same-side: -0.0053 ± 0.021, N = 101, P = 0.80; opposite-side: -0.0031 ± 0.020, N = 101, P = 0.88) or Empty (same-side: 0.0075 ± 0.014, N = 130, P = 0.59; opposite-side: 0.0012 ± 0.015, N = 130, P = 0.94). The same-side correlation was significantly higher than the opposite-side one under Demo (P = 0.0020, two-sided *Paired t*-test), but not under Object (P = 0.89) or Empty (P = 0.62; **Figure 4C**).

To verify the validity of this method, we performed the same analysis on the activities of ACC cells and CA1 ensembles during self-running in the maze (**Figure 4D**). The mean same-side correlation was significant under all conditions (Demo: 0.041 ± 0.010, N = 202, $P = 4.9 \times 10^{-5}$, two-sided t-test compared to 0; Object: 0.045 ± 0.019, N = 101, P = 0.0091; Empty: 0.065 ± 0.013, N = 130, $P = 7.1 \times 10^{-7}$), but not the opposite-side correlation (Demo: -0.0081 ± 0.0094, N = 202, P = 0.80; Object: -0.039 ± 0.015, N = 101, P = 0.99; Empty: 0.019 ± 0.013, N = 130, P = 0.084). The same-side correlations were also significantly higher than the opposite-side ones under all conditions (Demo: $P = 2.2 \times 10^{-14}$, two-sided *Paired t*-test; Object: $P = 9.1 \times 10^{-10}$; Empty: $P = 2.5 \times 10^{-7}$). Because ACC selective cells and their same-side CA1 ensembles were activated together during self-running under all conditions, this result shows that the method correctly identified the expected ACC-CA1 interactions during self-running in the maze.

Our data thus show that ACC selective cells were temporarily correlated with CA1 place cells encoding the same maze trajectories during delay periods in the box. The result suggests an ACC-CA1 interaction during observation that is specific to the observed, and thus the future, spatial trajectories.

Interaction between ACC cells and CA1 place cells around sharp-wave ripples

Since the replay of place cells within sharp-wave ripples (SWRs) may be involved in planning future spatial trajectories (Carr et al., 2011; Jadhav et al., 2012; Pfeiffer and Foster, 2013; Wu et al., 2017), we asked whether ACC cells interacted with CA1 place cell activities within SWRs in the observation box.

We examined firing activities of ACC cells, along with their CA1 ensembles, during water consumption periods in the box, because SWRs in the box primarily occurred during water consumption when individual place cells in CA1 ensembles fired spikes in population bursts. As shown in **Figure 5A**-**B**, an example ACC right-selective cell and its CA1 same-side (right) ensemble tended to activate together with SWRs during the water consumption periods on the same side of their selectivity (right trials) in the box.

We quantified the firing rates of ACC cells, as well as their associated CA1 ensembles within SWRs, during the water consumption period of each trial in the box. Overall, both ACC cells and CA1 ensembles had higher firing rates on the same side of their selectivity than the opposite-side under Demo, but not under Object or Empty (**Figure S5**). We computed the correlation between the trial-by-trial firing rates of each ACC cell and those of its same- or opposite-side CA1 ensemble (same-side or opposite-side correlation). For the example ACC cell in **Figure 5A**, its same-side correlation was significant (R = 0.27, P = 0.047, *Pearson's r*), but not its opposite-side one (R = 0.00033, P = 0.50), indicating that, when the cell displayed a high rate in the water consumption period of a trial (e.g., a right trial), the CA1 same-side (right) ensemble, but not the CA1 opposite-side (left) ensemble, was also activated with a high rate in the same trial (**Figure 5C**).

Averaging over all ACC cells (**Figure 5D**), we found that the mean same-side correlation under Demo was significantly higher than 0 (0.035 ± 0.019, N = 202, P = 0.04, one-sided *t*-test compared to 0). The mean opposite-side correlation showed a trend toward significance (0.028 ± 0.019, N = 202, P = 0.08), likely due to a general interaction between CA1 activities around SWRs with prefrontal cortical areas including ACC, as shown in previous studies (Jadhav et al., 2016; Remondes and Wilson, 2015). However, the same-side correlation was significantly higher than the opposite-side one (P = 0.047, one-sided *Paired t*-test). In contrast, the same- and opposite-side correlations were not significantly higher than 0 and not significantly different from each other under Object (same: -0.047 ± 0.028, N = 101, P = 0.95, one-sided *t*-test compared to 0; opposite: -0.045 ± 0.028, P = 0.94, one-sided *t*-test compared to 0; P = 0.68, one-sided *Paired t*-test between same and opposite) or Empty (same: -0.011 ± 0.020, N = 130, P = 0.70, one-sided *t*-test compared to 0; opposite: -0.0088 ± 0.021, P = 0.66, one-sided *t*-test compared to 0; P = 0.65, one-sided *Paired t*-test between same and opposite). The result suggests an ACC-CA1 interaction associated with SWRs, following their interaction during observation but prior to self-running, that is specific to the observed, and thus the subsequent future, spatial trajectories.

ACC activities during observation are associated with specific spatial contents of CA1 place cell activities within sharp-wave ripples

Given the specific ACC-CA1 interaction during delay periods and around SWRs afterward, we next asked how activities of ACC selective cells during observation of a trial were related to later CA1 activities within SWRs of the same trial.

We examined the firing activities of ACC cells during delay periods and their associated same- and opposite-side CA1 ensembles in SWRs during water consumption in the box (**Figure 6A-D**) and computed their firing rates in each trial. As shown in **Figure 6E**, the trial-by-trial firing rates in delay periods of an example ACC cell were correlated with the rates of its same-side CA1 ensemble in SWRs (same-side correlation: $R = 0.24$, $P = 0.05$, *Pearson's r*), but not with its opposite-side CA1 ensemble (opposite-side correlation: $R = 0.065$, $P = 0.34$), indicating that a high (low) firing rate of the ACC cell in a trial was associated with a high (low) rate of its CA1 same-side ensemble (not the opposite-side ensemble).

Averaging over all ACC cells (**Figure 6F**), we found that the mean same-side correlation under Demo in this case was significant (0.051 ± 0.015, $N = 202$, $P = 5.7 \times 10^{-4}$, two-sided *t*-test compared to 0). The mean opposite-side correlation again showed a trend toward significance (0.028 ± 0.014, $N = 202$, $P = 0.051$), but was significantly lower than the same-side one ($P = 3.3 \times 10^{-10}$, two-sided *Paired t*-test). In contrast, the same- and opposite-side correlations were not significant and not significantly different from each other under Object (same: -0.030 ± 0.026, $N = 101$, $P = 0.25$, two-sided *t*-test compared to 0; opposite: -0.029 ± 0.026, $P = 0.26$, two-sided *t*-test compared to 0; $P = 0.87$, two-sided *Paired t*-test between same and opposite) or Empty (same: -0.004 ± 0.019, $N = 130$, $P = 0.83$, two-sided *t*-test compared to 0; opposite: 0.0012 ± 0.020, $P = 0.95$, two-sided *t*-test compared to 0; $P = 0.35$, two-sided *Paired t*-test between same and opposite). In addition, we found a strong correlation between activities of ACC selective cells during observation and their activities during water consumption afterward in the box (**Figure S6**), suggesting a continuation of ACC cell activation in the box from observation to later water consumption of the same trial.

Finally, we analyzed how ACC activities during observation were related to the precise spatial contents encoded by CA1 replay activities within SWRs. For each of those SWRs identified as a replay event, we determined which of the maze trajectories was replayed, by Bayesian decoding using place cell templates during self-running (**Figure 7A**) (Davidson et al., 2009; Karlsson and Frank, 2009; Zhang et al., 1998). We computed a correlation between the trial-by-trial firing rate of an ACC cell during delay periods and the number of replays for the inbound or outbound trajectory template on the same- or opposite-side of its selectivity (same- or opposite-side, inbound or outbound template).

As shown in **Figure 7B**, the firing rate of an example ACC cell was significantly correlated with the number of replays for the same-side inbound template (same-side inbound correlation: $R = 0.45$, $P = 0.0012$, *Pearson's r*), but not for the opposite-side inbound one (opposite-side inbound correlation: $R = -0.28$, $P = 0.97$), indicating that a high (low) firing rate of the ACC cell during observation in a trial was associated with a high (low) number of replays for its CA1 same-side, but not the opposite-side, inbound template.

Averaging over all ACC selective cells (**Figure 7C**), we found that the mean same-side inbound correlation under Demo was significantly higher than 0 (0.028 ± 0.015, $N = 202$, $P = 0.034$, one-sided *t*-test compared to 0), but not the opposite-side inbound correlation (-0.012 ± 0.015, $N = 202$, $P = 0.78$). The same-side inbound correlation was also significantly higher than the opposite-side one ($P = 0.048$, one-sided *Paired t*-test). Under the control condition of Object, the same- and opposite-side inbound correlations were

not significantly higher than 0 and not significantly different from each other (same: -0.018 ± 0.023, N = 101, P = 0.79, one-sided t-test compared to 0; opposite: -0.0024 ± 0.023, P = 0.54, one-sided t-test compared to 0; P = 0.68, one-sided *Paired* t-test between same and opposite). Under Empty, such same-side correlation was even significantly lower than 0 and lower than the opposite-side correlation (same: -0.028 ± 0.016, N = 130, P = 0.044, one-sided t-test compared to 0; opposite: 0.014 ± 0.019, P = 0.23, one-sided t-test compared to 0; P = 0.040, one-sided *Paired* t-test between same and opposite). Thus, high ACC activities during observation were associated with high activities of same-side CA1 ensembles within SWRs only under Demo, but not under the two control conditions. In contrast, such association did not occur between ACC activities and opposite-side CA1 ensembles under all the conditions.

Interestingly, the difference in the ACC-CA1 association between the same-side and opposite-side was less evident for outbound templates (**Figure 7D**). The mean same-side outbound correlation under Demo was still significantly higher than 0 (0.027 ± 0.013, N = 202, P = 0.020, one-sided t-test compared to 0), but not the opposite-side (0.0092 ± 0.012, N = 202, P = 0.23). However, the difference between the same- and opposite-side correlations did not reach a significance level (P = 0.12, one-sided *Paired* t-test). The same- and opposite-side outbound correlations were not significantly higher than 0 and not significantly different from each other under Object (same: -0.0082 ± 0.019, N = 101, P = 0.67, one-sided t-test compared to 0; opposite: -0.028 ± 0.021, P = 0.90, one-sided t-test compared to 0; P = 0.19, one-sided *Paired* t-test between same and opposite) or Empty (same: -0.00082 ± 0.016, N = 130, P = 0.52, one-sided t-test compared to 0; opposite: -0.0071 ± 0.017, P = 0.67, one-sided t-test compared to 0; P = 0.39, one-sided *Paired* t-test between same and opposite).

Taken together, our data support that activation of ACC cells selective to the observed trajectories during observation is associated with the later activation of CA1 ensembles in SWRs selective to the same trajectories. More specifically, such ACC activation during observation is associated with a bias of CA1 place cell replay toward the observed trajectories, especially inbound ones, later in the same trial in the box. Given that the replay for inbound trajectories predicts the trajectories during subsequent self-running in the maze (Mou et al., 2022), our result here suggests that ACC activities during observation in the box influence subsequent spatial decisions in the maze through their bias on CA1 replay in SWRs.

DISCUSSION

We have analyzed activities of ACC cells and their interactions with CA1 place cells in the oSWM task. We found that many ACC cells, selective to the left or right side of the T-maze during self-running, are also activated during observation (delay periods) with same-side selectivity in the observation box. Such ACC same-side selectivity is reduced in error trials. The activities of ACC selective cells are correlated with those of CA1 same-side ensembles during observation and during water consumption afterward. In addition, the ACC activities during observation are correlated with CA1 activities within sharp-wave ripples and bias the spatial contents of CA1 replay in the box toward future trajectories in the maze. These results reveal the selective activation patterns of ACC neurons during ongoing observation and how they interact with hippocampal place cells to guide

subsequent spatial behavior.

The activation of ACC selective cells during observation supports a specific functional role of ACC in oSWM. ACC cells are selective to particular trajectories or segments of the maze during self-running, consistent with the relatively coarse spatial responses of prefrontal cortical neurons (compared to CA1 place fields) in previous studies (Jadhav et al., 2016; Jones and Wilson, 2005; Mashhoori et al., 2018; Remondes and Wilson, 2015; Siapas et al., 2005). It is unlikely that these ACC cells encode spatial locations similarly to place cells. Given that previous studies show that ACC activities are modulated by valence, value, or decision outcomes (Caracheo et al., 2018; Hillman and Bilkey, 2010; Kane et al., 2022; Mashhoori et al., 2018; Monosov, 2017), it is possible that the ACC selective activities in the maze reflect the reward or value associated with the spatial segments or trajectories being traveled. A major finding in this study is that these ACC cells, selective in the maze, are also selective to the same side of the observation box during delay periods. The oSWM task here utilizes a “same-side” rule that the OB learns to run the same-side trajectories of the Demo in the maze, which by design is to include the two behavioral phases, observation and imitation, of the classical social learning theory (Bandura, 1997) in a single trial of the working memory task. The same-side selectivity of ACC cells indicates that, when the OB performs the task correctly in each trial, the ACC cells selective to the correct future trajectories during self-running are already activated during observation, but not those selective to the trajectories on the opposite side. Such same-side selectivity only occurs with the presence of the Demo, not under the control Object or Empty condition, and it is reduced in error trials, suggesting that the selective activation of ACC cells during observation is not simply due to the OB moving to the same-side in the box. Our finding thus supports the following hypothesis: ACC neurons coding the value of trajectories in the maze during self-running are also activated during observation, cued by the observed Demo's action, to assign a "vicarious value" to the correct future trajectories.

Our results also suggest that hippocampal place cells may play a functional role different from that of ACC cells in oSWM. CA1 place cells selective to the left or right side of the maze during self-running do not display same-side selectivity during observation in the box. Thus, the observation-induced neural activities relevant to spatial decisions appear to be more distinguishable in ACC neurons than in CA1 neurons. CA1 place cells may be more important in the water consumption period when SWRs occur. Evidence exists that CA1 activities within SWRs, especially the replay events, are involved in the planning of immediate future trajectories (Carr et al., 2011; Jadhav et al., 2012; Pfeiffer and Foster, 2013; Wu et al., 2017). Indeed, remote replay of inbound trajectories in the box can be used to predict the subsequent choice in the maze in this oSWM task (Mou et al., 2022). Therefore, it is possible that the CA1 place cell activities within SWRs in the box plan for the future trajectories to run in the maze.

How does the value information encoded in ACC cells during observation lead to a spatial plan later encoded in CA1 place cell activities within SWRs? First, our data show that the activities of ACC selective cells and their CA1 same-side ensembles are temporarily correlated during delay periods, suggesting a functional interaction between ACC and CA1 cells during observation. Second, our data also show that the ACC activation during delay periods continues to the water consumption period in the box, when frequent SWRs

occur. Indeed, activities of ACC selective cells and their CA1 same-side ensembles in SWRs are correlated during water consumption in the box, and activities of CA1 same-side and opposite-side ensembles within SWRs become distinguishable. This ACC-CA1 interaction is consistent with previous studies that demonstrate an ACC-CA1 correlation around SWRs in different behavioral tasks (Jadhav et al., 2016; Mashhoori et al., 2018; Remondes and Wilson, 2015). The correlation can be mediated by the direct (Cenquizca and Swanson, 2007; Rajasethupathy et al., 2015) or indirect (Bubb et al., 2017; Sakata et al., 2019) anatomical connections between the hippocampus and medial prefrontal cortex (mPFC) including ACC. It is believed that the occurrence of SWRs marks an internal hippocampal state for planning, memory recall, or consolidation (Buzsaki, 2015). Unlike the active state during observation when CA1 cells actively respond to input originated from sensory cortices, CA1 cells during SWRs may be driven more internally from prefrontal areas including ACC (Wang and Ikemoto, 2016). Finally, our data also demonstrate that the activation of ACC selective cells during observation in a trial is accompanied by the preferential activation of their CA1 same-side ensembles and biases CA1 replay toward same-side trajectories prior to self-running. Taken together, the continued ACC activation from delay periods to water consumption periods and the ACC-CA1 interaction around SWRs enable the ACC cells selective to the future trajectories to bias the CA1 replay in the box, which in turn plans for subsequent self-running on the same trajectories in the maze.

In summary, our study of ACC cells and their interactions with hippocampal place cells in the oSWM task provides evidence that observing the action of a social subject activates specific ACC cells that encode value information involved in self decisions. These ACC cells interact with CA1 place cells for planning subsequent spatial behavior. ACC cells are known to be involved in observational learning (Allsop et al., 2018; Burgos-Robles et al., 2019; Jeon et al., 2010; Olsson and Phelps, 2007) and decision making (Hillman and Bilkey, 2010; Kane et al., 2022). Our study thus provides a link between these properties of ACC cells and reveals a specific functional role for their interaction with CA1 place cells in observational learning of spatial navigation.

METHODS

Animal

Sixteen 4 – 10 months male Long-Evans rats (Charles River Laboratories), with a weight of 400 – 600 g, were used in this study. Among them, 10 rats were used in the lesion experiment and 6 were used for the electrophysiological recording experiment. All experimental procedures followed the guidelines from the US National Institute of Health and were approved by the Institutional Animal Care and Use Committee at Baylor College of Medicine.

Apparatus

Our behavioral apparatus consisted of a small observation box and a continuous T-maze with a resting box. Briefly, the trapezoidal observation box was placed ~30 cm away from the choice point of the T-maze. Both the observation box and the T-maze were elevated ~50 cm above the floor. There were 2 water ports mounted on two side walls of the observation box and 2 at the T-maze. An animal's nosepoke at a water port triggered

water delivery through peristaltic water pumps if correct behavioral response was performed.

Behavioral procedure

Animals were water-deprived several days before the training started while food was available ad libitum at all times. Animals' weight was maintained at > 85% of the ad libitum level. Every rat in this study was first trained as an observer (OB) in the oSWM task to reach a criterion performance (>70% correct trials in the maze for at least 2 consecutive days). The electrophysiological recording or behavioral testing in the lesion experiment was then performed in daily sessions of ~90 minutes, each with a well-trained OB performing the oSWM task for ~40 trials.

Three behavioral conditions were used in the electrophysiology experiment. 1) *Demo*. This was the standard experimental condition. In each trial of the task, a well-trained demonstrator (Demo) randomly chose the left or right side (outbound trajectory) and then poked for water reward in the T-maze, while a well-trained OB observed the Demo and was rewarded with water if the OB poked on the same side in the observation box as the Demo's in the maze within 10 s of the Demo's first poke. The Demo returned via a left or right sidearm (inbound trajectory) and was confined in a rest box. The OB was transported to the T-maze at the beginning of the central arm and rewarded with water if the animal ran to the same side of the maze (outbound trajectory) as the Demo did (same-side rule). The OB returned via the same sidearm (inbound trajectory) as the Demo did and was transported back to the observation box before the next trial started. An error trial in this case was when the OB ran to the opposite-side of maze to the Demo's and was not rewarded in the maze. 2) *Object*. In each trial under this condition, the Demo was replaced by a moving object (10 cm × 20 cm black rectangle plastic block attached to the end of a 1.5 m wood pole). The movement of the object mimicked the Demo's movement in the T-maze. The moving object triggered the water ports and then remained at the reward location for a similar duration as the Demo rat did under the Demo condition. A trial was considered correct (an error) if the OB's choice in the maze was the same (or opposite-side) water port the object activated. 3) *Empty*. In each trial under this condition, the Demo was removed and the T-maze was left empty. A manually controlled wood pole triggered the water ports every ~2 min and remained at the reward location for a similar duration as the Demo rat did under the Demo condition. A trial was considered correct (or an error) if the OB chose the same (or opposite-side) water port activated manually.

Only one condition was conducted per day. When multiple conditions were used for the same OB, the OB was re-trained before the next condition under the standard Demo condition if the OB's performance in the maze was below the criterion under the previous condition.

Surgery for electrophysiological recording

Six well-trained OBs were surgically implanted with a hyperdrive consisting of 22 independently movable tetrodes and two reference electrodes, similarly as in previous studies (Haggerty and Ji, 2015; Mou et al., 2022). The electrodes targeted two regions: the right dorsal anterior cingulate cortex at coordinates anteroposterior (AP) 1.6 mm and mediolateral (ML) 1.0 mm from the Bregma, and the right dorsal hippocampal CA1 region at coordinates AP -3.8 mm, ML 2.4 mm. Animals were anesthetized using isoflurane (0.5

– 3%) and the hyperdrive was fixed to the rat skull through dental cement and anchoring screws.

Recording procedure

Within 2–3 weeks following the surgery, hippocampal tetrodes were slowly advanced to the CA1 pyramidal layer until characteristic sharp-wave ripples (SWRs) were observed (Buzsaki et al., 1992). ACC tetrodes were left in the cortex. One tetrode placed in the white matter above the CA1 and one silent tetrode in ACC were selected as the reference tetrode for CA1 and ACC, respectively. Recording started only after the tetrodes had not been moved for at least 24 hours.

Within about 2 - 3 weeks after the surgery, the OBs were accustomed to the hyperdrive and re-trained back to the criterion performance under the standard Demo condition (under Demo). Afterward, each OB was recorded while performing the oSWM task for 5 - 11 consecutive daily sessions under Demo, Object or Empty, as described above.

Lesion experiment

Ten well-trained OBs were used for the lesion experiment to examine whether the oSWM task was ACC-dependent. Rats were randomly assigned to a lesion (*N* = 5) or a control group (*N* = 5). For the lesion group, neurotoxic lesions in ACC were made by infusing N-methyl-D-aspartate (NMDA, Sigma-Aldrich, St. Louis, MO) in a phosphate-buffered saline (PBS) vehicle (20 μg/μL made by 100 mM PBS, pH = 7.4), bilaterally at a rate of 0.2 μL/minute to each of three ACC sites per hemisphere using a microinfusion pump (KD Scientific, Holliston, MA) and a 10-μL Hamilton syringe (Hamilton, Reno, NV). The coordinates of the infusion sites were: [AP 2.1 mm, ± ML 0.6 mm, -2.5 mm ventral to the dura (DV)], [AP 1.2 mm, ± ML 0.6 mm, DV -2.5 mm], [AP 0.3 mm, ± ML 0.6 mm, DV -2.5 mm]. A total of 0.2 μL was injected at each site and the syringe was left at each infusion site for 3 minutes. For the control group, 0.2 μL PBS vehicle alone was similarly infused to each of the 6 coordinates. After the animals fully recovered from the surgery (~14 days), they were tested in the oSWM task under the standard Demo condition.

Histology

To verify the recording and infusion sites, all OBs in the recording and lesion experiments were euthanized (pentobarbital, 150 mg/kg) and subjected to histology. For the recorded animals, a small lesion at each recoding site was generated by passing a 30-μA current for 10 s on each tetrode. Brain tissues were fixed (10% formaldehyde solution overnight) and sectioned at 90-μm thickness. Brain sections were stained using 0.2% Cresyl violet and cover-slipped for storage. Tetrode recording locations were identified by matching the lesion sites with tetrode depths and their relative positions.

Data acquisition

A Digital Lynx acquisition system (Neuralynx, Bozeman, MT) was used to record spikes and local field potential (LFP) signals, as described previously (Haggerty and Ji, 2015; Mou and Ji, 2016; Wu et al., 2017). A 60-μV threshold was set for spike detection. Spike signals above this threshold were sampled at 32 kHz and digitally filtered between 600 Hz and 9 kHz. LFP signals were sampled at 2 kHz and filtered between 0.1 Hz – 1 kHz. The head and body center positions of each animal were tracked at 30 Hz with a resolution of approximately 0.1 cm by the EthoVision XT system (Noldus, Leesburg, VA).

Behavioral quantification

We quantified each OB's behavioral performances in the observation box and in the T-maze. Briefly, the performance in the box was quantified by a poke performance curve for each session, which was the normalized poke rate at each 0.25-s time bin in the box, aligned relatively to the corresponding Demo's poking time in the maze in each trial (time 0). The performance in the maze was quantified by the percentage of correct trials for each session.

Cell inclusion

Spikes detected using Neuralynx were sorted into single units (single cells) off-line, using a custom software (xclust, M. Wilson at MIT, available at GitHub: https://github.com/wilsonlab/mwsoft64/tree/master/src/xclust). Some cells might be repeatedly sampled across sessions since we did not track cell identities across multiple recording sessions. A total of 1049 ACC cells and 2102 CA1 cells were obtained in 44 sessions from 6 OB rats. Among the CA1 cells, 1226 were classified as putative CA1 pyramidal neurons active (mean firing rate between 0.4 and 10 Hz) in the T-maze. These active CA1 cells and all ACC cells were included in the analysis of neural data.

ACC selective cell, selectivity index (SI), and SI correlation

For each ACC cell, we computed its firing rate on the left or right side of the maze during self-running for each trial, by dividing the number of spikes occurring during active running, with the stopping periods (velocity < 5 cm/s for > 3 s) excluded, on the outbound and inbound trajectory combined for each side over the total amount of running time. A cell was classified as a selective cell if its mean rates on the left and on the right side of the maze averaged over all correct trials were significantly different ($P < 0.05$, two-sided *t*-test).

Further analysis on ACC was performed only on ACC selective cells unless otherwise specified. For each such ACC selective cell, we also computed the firing rates during the delay period of each trial in the observation box, defined as the 2 s before the first correct (rewarded) poke in the box, and considered it selective in the box if its mean rates during delay periods between left and right correct trials were significantly different. A cell was determined to have same- or opposite-side selectivity if it was selective in the box to the same side as or different side from that in the maze.

To quantify the significance of the percentage of ACC cells with same- or opposite-side selectivity (among all ACC selective cells), we randomized every cell's rates during delay periods of left or right trials and recounted the percentage of cells with same- or opposite-side selectivity. This was repeated 1000 times and a (chance-level) distribution of the resulting 1000 percentage numbers was obtained. The actual number was z-scored relative to the chance-level distribution with its significance determined by the *Z*-test.

For every cell, we also computed a selectivity index (SI), given its mean rates on the left (FR_{left}) or right (FR_{right}) side in the maze or box, as

$$SI = \frac{FR_{right} - FR_{left}}{FR_{right} + FR_{left}}. \qquad (1)$$

To assess the level of same-side selectivity at the population level, we correlated the SIs in the box for all ACC selective cells and their SIs in the maze, with the significance determined by *Pearson's* correlation coefficient *r*. The same analysis was applied to individual CA1 cells active in the maze to assess their same-side selectivity during delay periods in the box.

CA1 sharp-wave ripple (SWR) detection

SWRs were detected as population burst events (PBEs) from the CA1 multiunit activity (MUA), as in previous studies (Diba and Buzsaki, 2007; Mou et al., 2022; Wu et al., 2017). In each session, all putative spikes recorded by all CA1 tetrodes were binned in 10 ms time bins. Spike counts in each bin were counted and smoothed by a Gaussian kernel with a σ of two bins and standardized from 0 to 1. A PBE was defined as a time period such that the standardized peak MUA spike counts in this period exceeded a threshold of 0.35, and the MUA spike counts at the start and end times exceeded a threshold of 0.15. Adjacent PBEs with a gap < 30 ms were combined.

CA1 place cell ensembles and replay detection

For each CA1 cell active during self-running in the T-maze, we constructed its firing rate curves on the 4 maze trajectories (left/right, inbound/outbound). For each trajectory of a session, we then constructed a place cell template. A CA1 cell was eligible to be included in a template if its rate curve on the trajectory had a peak firing rate of at least 3 standard deviations above its mean firing rate. A CA1 left or right ensemble was made of all cells in the inbound and outbound templates combined on the left or right side of the T-maze. The firing rate of an ensemble was computed by aggregating all spikes from all cells in the ensemble within a time bin.

We identified whether CA1 place cell activities within a SWR (PBE) replayed a place cell template on a trajectory by a Bayesian decoding method, as described in previous studies (Davidson et al., 2009; Karlsson and Frank, 2009; Mou et al., 2022; Wu et al., 2017; Zhang et al., 1998). Briefly, PBEs with at least 4 active CA1 template cells were defined as candidate PBEs for the template. For each candidate PBE, we assumed independent *Poisson* processes among the cells in the template and computed the posterior spatial probability distribution for each time bin (20 ms with a 10 ms overlapping step). The decoded position at each time bin was the location on the template trajectory with the maximum posterior probability. We then correlated the decoded positions and the time bin numbers. The *Pearson's* correlation coefficient *r* was compared to 1000 shuffle-generated coefficients, obtained by correlating the decoded positions with randomly shuffled time bin numbers 1000 times. The proportion of shuffle-generated coefficient values greater than the actual one gave the significance *P* value. A candidate PBE was considered a replay if $P < 0.05$.

Firing rate difference in error trials and during water consumption

For each ACC cell with same-side selectivity, we computed its firing rates during delay periods on its preferred (left or right) side in correct and error trials of a session, if the session contained at least 3 error trials on its preferred side (the OB rewarded on its preferred side in the box, but ran incorrectly to the opposite side in the maze). A firing rate difference index (DI) was defined similarly as in Eq. (1) above. The rate difference between correct and error trials was assessed at the population level by comparing the

764 mean DI among all ACC cells with same-side selectivity to 0 by two-sided *t*-test. The
765 same analysis was also applied to ACC cells with same-side selectivity in error trials
766 occurring on their non-preferred side (the OB rewarded on the non-preferred side of a cell
767 in the box, but ran incorrectly to the opposite side in the maze).
768
769 For each ACC cell, we also compared its firing rates on the same-side or opposite-side
770 of its selectivity during water consumption periods of a session, similarly by a firing rate
771 DI computed as in Eq. (1). The same was performed on CA1 activities during water
772 consumption. Since CA1 firing activities within and outside SWRs are considered to
773 reflect different behavioral states (Buzsaki, 2015; Buzsaki et al., 1992; Csicsvari et al.,
774 2000), we restricted our analysis on CA1 activities during water consumption within
775 SWRs. Since each individual CA1 cell only fired very few or no spikes, we combined all
776 spikes of cells in a CA1 ensemble within a SWR to obtain an aggregated firing rate. The
777 difference between mean rates within the SWRs occurring on the same and opposite side
778 of an ensemble in the observation box (left or right for CA1 left or right ensembles) was
779 quantified by a firing rate DI.
780
781 **Firing rate correlation**
782 To quantify ACC-CA1 interactions, we computed firing rate correlations between ACC
783 selective cells and their CA1 same- or opposite-side ensembles in the observation box.
784 During delay periods, we computed firing rates of each ACC selective cell in 200 ms time
785 bins. Given the relatively sparse firing of CA1 cells, to avoid the bias of correlation by
786 firing rate, we computed the rate of a CA1 ensemble by counting all the aggregated spikes
787 of all cells in the ensemble within each time bin. The binned firing rates of an ACC cell
788 and its CA1 same- or opposite-side ensemble of all delay periods in a session were
789 correlated by *Pearson's* correlation coefficient to quantify the temporal correlation
790 between the ACC cell and the CA1 ensemble selective to the same- or opposite-side of
791 its selectivity.
792
793 During water consumption, we isolated spikes of CA1 ensembles within SWRs, for the
794 same reason that spikes within and outside SWRs reflect different behavioral states, and
795 computed their rates in each trial. We also computed the rate of each ACC selective cell
796 during the entire water consumption period in each trial, without considering specific time
797 periods since no specific activity patterns like CA1 population bursts in SWRs were
798 observed. For all trials in a session, the trial-by-trial firing rates of an ACC cell were
799 correlated with those of its CA1 same- or opposite-side by *Pearson's r*. A significant, high
800 value of such trial-by-trial correlation means that, when an ACC cell selective to the left
801 or right side of the maze fired with a high (or low) firing rate during the water consumption
802 period of a trial, the CA1 ensemble on the same-side of the maze was also activated with
803 a high (or low) rate within SWRs in the same period of the same trial.
804
805 Similarly, this trial-by-trial correlation was also used to quantify the relation between the
806 activity of an ACC selective cell during the delay period of a trial and its rate during the
807 water consumption or the rate of its CA1 same/opposite-side ensemble within SWRs
808 during the water consumption of the same trial. In addition, the trial-by-trial firing rates of
809 an ACC cell during delay periods were also correlated with the trial-by-trial numbers of
810 replay for the inbound or outbound trajectory template during water consumption.
811

Statistical analysis

Sample sizes were decided based on standards in the field. No sample-size calculations were performed prior to experimentation. Criteria for excluding individual cells or sessions from analyses were detailed above. Animals (OBs) were not allocated into experimental conditions completely randomly since all animals need to be trained with a Demo. Therefore, the Demo condition was always tested first before animals were assigned to other behavioral conditions. Investigators and animals were not blind to the condition allocation during data collection because the setup configurations and experimental conditions were evident to both investigators and animals by design. Analysis tools and codes were automated and applied to different conditions uniformly, therefore blinding was not relevant.

All statistical analyses were performed using MATLAB functions. Statistical significance level was set at $P < 0.05$. Some specific statistical tests are described above. In general, for parametric analyses, values are reported as mean ± SEM. *Two-way ANOVA* was used for multiple comparisons followed by post-hoc *Fisher's* least significant difference test corrected by multiple comparisons. *Paired t*-test *or t*-test was used to compare between two groups or between a sample of values and a fixed value (e.g. 0). One-sided or two-sided comparison was specified wherever used. For non-parametric analyses, values are reported as median [25 percentile 75 percentile]. *Kruskal-Wallis* test followed by Dunn's test were used for multiple comparisons. *Wilcoxon rank-sum* test or *signed-rank* test was used to compare between two groups. All statistical methods and sample size (*N*) were detailed in the main text or figure legends wherever used.

Data and Code Availability

- All data reported in this study will be shared by the corresponding authors upon request.
- All custom code used in this study will be shared by the corresponding authors upon request.
- Any additional information required to reanalyze the data reported in this study is available from the lead contact upon request.

ACKNOWLEDGMENTS

We thank Ji lab members for discussions. We thank J. Chin lab for suggestions on lesion experiments. This work is supported by grants from the National Institute of Mental Health (R01MH106552 and R01MH112523 to D.J.).

AUTHOR CONTRIBUTIONS

Conceptualization, X.M. and D.J.; Methodology, X.M. and D.J.; Investigation, X.M.; Formal analysis, X.M. and D.J.; Visualization, X.M. and D.J.; Writing – original draft, X.M. and D.J.; Writing – review & editing: X.M. and D.J.; Supervision, X.M. and D.J.; Funding acquisition, D.J.

DECLARATION OF INTERESTS

The authors declare no competing interests.

REFERENCES

Allsop, S.A., Wichmann, R., Mills, F., Burgos-Robles, A., Chang, C.J., Felix-Ortiz, A.C., Vienne, A., Beyeler, A., Izadmehr, E.M., Glober, G.*, et al.* (2018). Corticoamygdala Transfer of Socially Derived Information Gates Observational Learning. Cell 173, 1329-1342 e1318.

Bandura, A. (1997). Social learning theory. (New York, General Learning Press).

Bubb, E.J., Kinnavane, L., and Aggleton, J.P. (2017). Hippocampal - diencephalic - cingulate networks for memory and emotion: An anatomical guide. Brain Neurosci Adv 1.

Burgos-Robles, A., Gothard, K.M., Monfils, M.H., Morozov, A., and Vicentic, A. (2019). Conserved features of anterior cingulate networks support observational learning across species. Neurosci Biobehav Rev 107, 215-228.

Buzsaki, G. (2015). Hippocampal sharp wave-ripple: A cognitive biomarker for episodic memory and planning. Hippocampus 25, 1073-1188.

Buzsaki, G., Horvath, Z., Urioste, R., Hetke, J., and Wise, K. (1992). High-frequency network oscillation in the hippocampus. Science 256, 1025-1027.

Caracheo, B.F., Grewal, J.J.S., and Seamans, J.K. (2018). Persistent Valence Representations by Ensembles of Anterior Cingulate Cortex Neurons. Front Syst Neurosci 12, 51.

Carr, M.F., Jadhav, S.P., and Frank, L.M. (2011). Hippocampal replay in the awake state: a potential substrate for memory consolidation and retrieval. Nature neuroscience 14, 147-153.

Carrillo, M., Han, Y., Migliorati, F., Liu, M., Gazzola, V., and Keysers, C. (2019). Emotional Mirror Neurons in the Rat's Anterior Cingulate Cortex. Curr Biol 29, 2104.

Cenquizca, L.A., and Swanson, L.W. (2007). Spatial organization of direct hippocampal field CA1 axonal projections to the rest of the cerebral cortex. Brain research reviews 56, 1-26.

Csicsvari, J., Hirase, H., Mamiya, A., and Buzsaki, G. (2000). Ensemble patterns of hippocampal CA3-CA1 neurons during sharp wave-associated population events. Neuron 28, 585-594.

Danjo, T., Toyoizumi, T., and Fujisawa, S. (2018). Spatial representations of self and other in the hippocampus. Science 359, 213-218.

Davidson, T.J., Kloosterman, F., and Wilson, M.A. (2009). Hippocampal replay of extended experience. Neuron 63, 497-507.

Diba, K., and Buzsaki, G. (2007). Forward and reverse hippocampal place-cell sequences during ripples. Nature neuroscience 10, 1241-1242.

Foster, D.J., and Wilson, M.A. (2006). Reverse replay of behavioural sequences in hippocampal place cells during the awake state. Nature 440, 680-683.

Haggerty, D.C., and Ji, D. (2015). Activities of visual cortical and hippocampal neurons co-fluctuate in freely moving rats during spatial behavior. eLife 4.

Harris, K.D., Csicsvari, J., Hirase, H., Dragoi, G., and Buzsaki, G. (2003). Organization of cell assemblies in the hippocampus. Nature 424, 552-556.

Heyes, C.M., Galef, Jr. B. G. (1996). Social learning in animals: the root of culture. (New York, Academic Press).

Hillman, K.L., and Bilkey, D.K. (2010). Neurons in the rat anterior cingulate cortex dynamically encode cost-benefit in a spatial decision-making task. J Neurosci 30, 7705-7713.

Jadhav, S.P., Kemere, C., German, P.W., and Frank, L.M. (2012). Awake hippocampal sharp-wave ripples support spatial memory. Science 336, 1454-1458.

Jadhav, S.P., Rothschild, G., Roumis, D.K., and Frank, L.M. (2016). Coordinated Excitation and Inhibition of Prefrontal Ensembles during Awake Hippocampal Sharp-Wave Ripple Events. Neuron 90, 113-127.

Jeon, D., Kim, S., Chetana, M., Jo, D., Ruley, H.E., Lin, S.Y., Rabah, D., Kinet, J.P., and Shin, H.S. (2010). Observational fear learning involves affective pain system and Cav1.2 Ca2+ channels in ACC. Nature neuroscience 13, 482-488.

Johansen, J.P., Fields, H.L., and Manning, B.H. (2001). The affective component of pain in rodents: direct evidence for a contribution of the anterior cingulate cortex. Proceedings of the National Academy of Sciences of the United States of America 98, 8077-8082.

Jones, M.W., and Wilson, M.A. (2005). Theta rhythms coordinate hippocampal-prefrontal interactions in a spatial memory task. PLoS Biol 3, e402.

Kane, G.A., James, M.H., Shenhav, A., Daw, N.D., Cohen, J.D., and Aston-Jones, G. (2022). Rat Anterior Cingulate Cortex Continuously Signals Decision Variables in a Patch Foraging Task. J Neurosci 42, 5730-5744.

Karlsson, M.P., and Frank, L.M. (2009). Awake replay of remote experiences in the hippocampus. Nature neuroscience 12, 913-918.

Leggio, M.G., Molinari, M., Neri, P., Graziano, A., Mandolesi, L., and Petrosini, L. (2000). Representation of actions in rats: the role of cerebellum in learning spatial performances by observation. Proceedings of the National Academy of Sciences of the United States of America 97, 2320-2325.

Mashhoori, A., Hashemnia, S., McNaughton, B.L., Euston, D.R., and Gruber, A.J. (2018). Rat anterior cingulate cortex recalls features of remote reward locations after disfavoured reinforcements. eLife 7.

Meltzoff, A.N., Kuhl, P.K., Movellan, J., and Sejnowski, T.J. (2009). Foundations for a new science of learning. Science 325, 284-288.

Monosov, I.E. (2017). Anterior cingulate is a source of valence-specific information about value and uncertainty. Nat Commun 8, 134.

Mou, X., and Ji, D. (2016). Social observation enhances cross-environment activation of hippocampal place cell patterns. eLife 5.

Mou, X., Pokhrel, A., Suresh, P., and Ji, D. (2022). Observational learning promotes hippocampal remote awake replay toward future reward locations. Neuron 110, 891-902 e897.

O'Keefe, J., and Dostrovsky, J. (1971). The hippocampus as a spatial map. Preliminary evidence from unit activity in the freely-moving rat. Brain research 34, 171-175.

Olsson, A., and Phelps, E.A. (2007). Social learning of fear. Nature neuroscience 10, 1095-1102.

Omer, D.B., Maimon, S.R., Las, L., and Ulanovsky, N. (2018). Social place-cells in the bat hippocampus. Science 359, 218-224.

Pfeiffer, B.E., and Foster, D.J. (2013). Hippocampal place-cell sequences depict future paths to remembered goals. Nature 497, 74-79.

Rajasethupathy, P., Sankaran, S., Marshel, J.H., Kim, C.K., Ferenczi, E., Lee, S.Y., Berndt, A., Ramakrishnan, C., Jaffe, A., Lo, M.*, et al.* (2015). Projections from neocortex mediate top-down control of memory retrieval. Nature 526, 653-659.

Remondes, M., and Wilson, M.A. (2015). Slow-gamma Rhythms Coordinate Cingulate Cortical Responses to Hippocampal Sharp-Wave Ripples during Wakefulness. Cell Rep 13, 1327-1335.

Sakata, H., Kim, Y., Nejime, M., Konoike, N., Miyachi, S., and Nakamura, K. (2019). Laminar Pattern of Projections Indicates the Hierarchical Organization of the Anterior Cingulate-Temporal Lobe Emotion System. Front Neuroanat 13, 74.

Schneider, K.N., Sciarillo, X.A., Nudelman, J.L., Cheer, J.F., and Roesch, M.R. (2020). Anterior Cingulate Cortex Signals Attention in a Social Paradigm that Manipulates Reward and Shock. Curr Biol 30, 3724-3735 e3722.

Siapas, A.G., Lubenov, E.V., and Wilson, M.A. (2005). Prefrontal phase locking to hippocampal theta oscillations. Neuron 46, 141-151.

Wang, D.V., and Ikemoto, S. (2016). Coordinated Interaction between Hippocampal Sharp-Wave Ripples and Anterior Cingulate Unit Activity. J Neurosci 36, 10663-10672.

Wilson, M.A., and McNaughton, B.L. (1993). Dynamics of the hippocampal ensemble code for space. Science 261, 1055-1058.

Wu, C.T., Haggerty, D., Kemere, C., and Ji, D. (2017). Hippocampal awake replay in fear memory retrieval. Nature neuroscience 20, 571-580.

Zhang, K., Ginzburg, I., McNaughton, B.L., and Sejnowski, T.J. (1998). Interpreting neuronal population activity by reconstruction: unified framework with application to hippocampal place cells. Journal of neurophysiology 79, 1017-1044.

FIGURE LEGENDS

Figure 1. OB performances in the observation box and in the maze depended on ACC.

(**A**) Behavioral apparatus consisting of an observation box (top), a continuous T-maze and a rest box (bottom). Red: reward site (water port); arrow: running direction. OB/Demo: observer/demonstrator rat.

(**B**) Coronal brain sections after NMDA and vehicle infusion. Arrow: lesion in ACC. Number: anteroposterior coordinate from the Bregma.

(**C**) Average (mean ± SEM) poke performance curves of OBs in the box for the 3 sessions before (Before) and the first 3 testing sessions 2 weeks after NMDA or vehicle infusion (After).

(**D**) Maze performances of OBs in each of Before and After sessions. Thin/thick line: individual rat/average performance.

***: $P < 0.001$, **: $P < 0.01$, *: $P < 0.05$, n.s.: not significant (same for all figures).

Figure 2. ACC selective cells were activated during delay periods in the observation box.

(**A**) Spike raster of an ACC left- (top) and an ACC right-selective (bottom) cell on the left (magenta) and right (blue) sides of the T-maze, and their average firing rates along the (linearized) trajectories on the two sides (right curves). Each tick is a spike. Each row is a trial. Color markers show maze landmarks: choice point (CP), reward site (R), end of

side-arm (End). The two cells were from two different sessions. Error trials (top: 2 left and 4 right; bottom: 0) are excluded.

(**B**) Similar to (**A**), but for the same two cells during the 2-s delay period of each trial in the box (dash line: time 0 – first rewarded poke in the box). Note the higher rate on the same side of each cell's selectivity.

(**C**) Trial-by-trial firing rates of the same two cells in (**A**-**B**) during running on the left/right side of the maze and during delay period on the left/right side of the box. Note the similar selection indices (SIs, numbers) in the maze and in the box.

(**D**) SIs in the maze and in the box for all ACC selective cells under Demo, Object and Empty. Each dot is a cell. Black line: liner regression between maze and box SIs. Colored dots: cells with significant same-side selectivity in the box on the left (magenta) or right (blue).

(**E**) Percentages of ACC cells with significant same-side selectivity in the box (left/right combined, red lines) under Demo, Object and Empty, compared to random distributions (black) obtained by shuffling each cell's firing rates among all delay periods of left/right trials.

See also Figure S1, S2.

Figure 3. ACC cells with same-side selectivity in the box were less activated during delay periods of error trials.

(A) Left: illustration of a correct and an error left trial (the Demo chose left in the maze). A trial was considered an error if the OB chose the opposite (right) side in the maze, after getting rewarded (on the left side) in the box. Red: reward site. Right: trial-by-trial spike raster (top) of an ACC left-selective cell (in both the maze and box) and firing rates of this ACC cell in each correct/error trial (bottom) during delay periods of an example session. Each tick represents a spike. Magenta/blue: spikes in correct/error trials. Red dash line: OB's poke time (time 0). Number: firing rate difference index (DI) between correct and error trials for this cell.

(**B**) Similar to (**A**), but for an ACC right-selective cell in correct and error right trials. Blue/magenta: correct/error trials.

(**C**) Comparison of ACC cell DIs described in (**A**-**B**) during delay periods on their preferred side under Demo, Object and Empty.

(**D**) Percentages of ACC cells with same-side selectivity in the box that had significantly higher firing rate during delay periods of correct than error trials on their preferred side (left-selective and right-selective cells combined, red lines) under Demo, Object and Empty, compared to their shuffle-generated distributions (black).

See also Figure S3.

Figure 4. Activities of ACC cells were correlated with those of CA1 same-side ensembles during delay periods in the box.

(**A**) Trial-by-trial spike raster of an example ACC right-selective cell and its associated CA1 left and right ensembles during delay periods of left (magenta) and right (blue) trials of a session. Each tick is a spike. Red dash line: time of first rewarded poke in the box (time 0).

(**B**) Firing rate cross-correlation between the example ACC cell and its associated CA1 ensemble in (**A**). Red/black curves: average values over all trials in the session. Shaded areas: SEM. Note the peak correlation around time lag 0 (dash line) between the ACC cell and its same-side CA1 ensemble.

(**C**) Average correlations (mean ± SEM, at time lag 0) during delay periods between ACC cells and their CA1 same- (red) and opposite-side (black) ensembles under Demo, Object and Empty. Note the significant same-side correlation under Demo, but not under Object or Empty.

(**D**) Similar to (**C**), but for correlations during running laps in the maze. Note the significant same-side correlation under all three conditions, as expected.

See also Figure S4.

Figure 5. Activities of ACC cells were correlated with those of CA1 same-side ensembles during water consumption in the box.

(**A**) Spike raster of an example ACC right-selective cell during water consumption in the box for a left and a right trial of a session. Each tick is a spike.

(**B**) CA1 LFPs filtered within the ripple band (top) and spike raster of CA1 cells in the left (middle) and right ensemble (bottom) during the same time periods in (**A**). Arrows: SWRs. Note the population bursts associated with SWRs.

(**C**) Correlation (*r*) between trial-by-trial firing rates of the example ACC cell and its CA1 same- and opposite-side ensemble within SWRs during water consumption in the session. Each dot is a trial.

(**D**) Average correlations (mean ± SEM) for all ACC selective cells and their CA1 same- and opposite-side ensembles, as computed in (**C**), under Demo, Object and Empty.

See also Figure S5.

Figure 6. Activation of ACC selective cells during delay periods was associated with subsequent activation of CA1 same-side ensembles within SWRs during water consumption in the box.

(**A**) Spike raster of an ACC right-selective cell during delay periods of left trials in an example session. Each tick is a spike. Red dash line: OB's first rewarded poke in the box (time 0).

(**B**) Spike raster of CA1 left and right ensembles within SWRs during water consumption periods of the same (left) trials in (**A**). Only spikes within SWRs of a 1 s window are shown for clarity.

(**C**-**D**) Similar to (**A**-**B**), but for the same ACC (right-selective) during delay periods and same CA1 ensembles during water consumption periods in the right trials of the same session.

(**E**) Correlation (*r*) between trial-by-trial firing rates of the ACC cell during delay periods and its CA1 same- or opposite-side ensembles within SWRs during water consumption in the session. Each dot represents a trial.

(**F**) Average correlations (mean ± SEM) for all ACC selective cells and their CA1 same- and opposite-side ensembles, as computed in (**E**), under Demo, Object and Empty.

See also Figure S6.

Figure 7. Activation of ACC selective cells during delay periods was associated with the replay of CA1 same-side ensembles during water consumption in the box.

(**A**) Spike raster (middle) of an example forward/reverse replay of the CA1 template cells corresponding to the right outbound/inbound trajectory (top). The Bayesian-decoded probability of trajectory positions at each time bin is shown at the bottom. x: decoded (peak probability) positions. Dashed line: replay order of spikes.

(**B**) Trial-by-trial correlation (*r*) between an example ACC cell's firing rate during delay periods and the number of replays for CA1 templates on the same- or opposite-side inbound trajectories of the ACC cell's selectivity. Each dot represents one trial.

(**C**) Average correlation values (mean ± SEM) for all ACC selective cells and the corresponding replay numbers for same- or opposite-side templates, as computed in (**B**), under Demo, Object and Empty. Note the higher same-side correlation under Demo, but not under Object or Empty.

(**D**) Similar to (**C**), but for outbound trajectories.

SUPPLEMENTAL INFORMATION

Figure S1. Behavior of OBs during delay periods in the observation box, related to Figure 2.

(**A**) Illustration of the delay time window of a trial: time interval between the Demo passing the T-maze choice point (CP) on a left (magenta) or right (blue) trajectory and the OB's first poke with reward at the corresponding water port in the box (not drawn proportionally).

(**B**) Distribution of the delay window duration for all trials of all recorded OBs under the Demo condition. Note the peak at 1.97 s.

(**C**) Top: an example OB's head direction within the 2 s (Start) delay period before first rewarded poke (End) in the box for a left and right trial. Head direction was computed in every 0.1 s time bin. Downward arrow shows the direction (270°) facing the T-maze.

Bottom: distribution of the OB's head direction in the 2 s delay periods of all trials in a session with left/right rewarded pokes. Number inside circle: radius length (count of time bins). Red rectangles: reward sites (at ~210°, 330°).

(**D**) Similar to (**C**), but for the OB's head position in the same left and right trial (top) and head position density during delay periods of all trials in the session. Bottom color bar: count of time bins. Gray trace: all head positions in the session.

Figure S2. ACC cells with opposite-side selectivity in the box were fewer than the chance level under Demo, related to Figure 2.

(**A**) Numbers of ACC selective cells (white) and corresponding percentages among all recorded ACC cells under Demo, Object and Empty.

(**B**) SIs in the maze and in the box for all ACC selective cells under Demo, Object, and Empty. The plots are the same as in **Figure 2D**, but now the colored dots highlight those left- (magenta) or right- (blue) selective cells in the maze that had significant opposite-side selectivity in the box.

(**C**) Percentages of ACC selective cells with significant opposite-side selectivity in the box (red lines) under Demo, Object and Empty, compared to their random distributions (black) obtained by shuffling each cell's firing rates among all delay periods of left and right trials in the box. Demo: 14%, $Z = -4.1$, $P = 2.1 \times 10^{-5}$, *Z*-test; Object: 27%, $Z = 0.47$, $P = 0.32$; Empty: 22%, $Z = -1.2$, $P = 0.89$.

Figure S3. ACC cells with same-side selectivity in the box did not differ in firing rate during delay periods between correct and error trials on their non-preferred side, related to Figure 3.

(**A**) Average DIs (mean ± SEM) of ACC cells with same-side selectivity in the box on their non-selective side between delay periods of correct and error trials under Demo, Object and Empty. The DIs were not significantly different from 0 (Demo: -0.051 ± 0.030, N = 44, P = 0.11, two-sided t-test; Object: 0.032 ± 0.021, N = 84, P = 0.13; Empty: -0.026 ± 0.016, N = 124, P = 0.11). There was a significant difference among the 3 conditions (*One-way ANOVA*: $F_{(1,251)}$ = 3.54, P = 0.030).

(**B**) Percentages of ACC cells with same-side selectivity in the box that had significantly higher rate during delay periods in correct trials on their non-preferred side (red, left-selective and right-selective cells combined) under Demo, Object and Empty, compared to shuffle-generated distributions (black). The percentage was not significant from the chance level under Demo (2.3%, Z = -0.77, P = 0.78, Z-test), Object (4.8%, Z = -0.0062, P = 0.50) or Empty (2.4%, Z = -1.2, P = 0.88).

Figure S4. CA1 cells with same-side selectivity in the box were not significantly different from the chance level, related to Figure 4.

(**A**) Firing rates of two example CA1 cells during running in each trial on the left/right side of the maze and during each delay period in the box. Note different SIs (numbers) between the maze and box. (Left-selective cell: Maze: P = 3.3 x 10^{-4}, two-sided t-test; Box: P = 0.11; Right-selective cell: Maze: P = 0.0022; Box: P = 0.15)

(**B**) SIs in the maze and in the box for all CA1 cells active in the maze under Demo, Object and Empty. Colored dots: cells with significant same-side selectivity in the box on the left (magenta) or right (blue). Black line: linear regression between the maze and box SIs. There was no significant correlation under any of the conditions (Demo: R = -0.10, P = 0.93, *Pearson's r*; Object: R = -0.025, P = 0.59; Empty: R = 0.061, P = 0.24).

(**C**) Percentages of CA1 cells with significant same-side selectivity in the box (left/right combined, red lines) under Demo, Object and Empty, compared to their distributions (black) obtained by random shuffling of each cell's firing rates among all delay periods of left/right trials. The actual percentage was not significantly different from the random distribution under any of the conditions (Demo: 23%, Z = -0.54, P = 0.70, Z-test; Object: 22%, Z = -1.3, P = 0.91; Empty: 24%, Z = -0.38, P = 0.65).

Figure S5. Activities of ACC selective cells and CA1 ensembles during water consumption in the box differed between same- and opposite-side of their selectivity, related to Figure 5.

(A) Trial-by-trial firing rates of a left-selective ACC cell during water consumption in the box on the same- and opposite-side of its selectivity in an example session. Each dot is a trial. Horizontal lines: mean values. Number: firing rate difference index (DI) between same- and opposite-side for this ACC cell.

(B) Average firing rate DIs over all ACC selective cells during water consumption under Demo, Object and Empty. The DIs were significantly higher than 0 under Demo (0.042 ± 0.013, N = 200, P = 9.1 x 10^{-4}, two-sided t-test), but not under Object (0.0053 ± 0.018, N = 99, P = 0.76) or Empty (-0.015 ± 0.018, N = 130, P = 0.41). There was a significant difference among the 3 conditions (*One-way ANOVA* test: $F_{(1,427)}$ = 4.0, P = 0.019).

(C-D) Similar to (**A-B**), but for firing rates of CA1 ensembles on the same- and opposite-side of ensembles. The average DIs in (**D**) were significantly higher than 0 under Demo (0.020 ± 0.0053, N = 19, P = 1.3 x 10^{-3}, , two-sided t-test), but not under Object (-0.011 ± 0.012, N = 11, P = 0.41) or Empty (0.0048 ± 0.0074, N = 13, P = 0.53). There

was a significant difference among the 3 conditions (*One-way ANOVA* test: $F_{(1,42)} = 3.9$, $P = 0.028$).

Figure S6. Activities of ACC selective cells during delay periods were correlated with their activities during water consumption periods in the box, related to Figure 6.

(**A**) Trial-by-trial correlation (*r*) between the firing rates of an example ACC cell during delay periods and during water consumption in all trials of a session. Each dot represents a trial.

(**B**) Average correlation values (mean ± SEM) for all ACC selective cells under Demo, Object and Empty. The correlations were significant under all the 3 conditions (Demo: 0.26 ± 0.019, $N = 200$, $P = 5.7 \times 10^{-32}$, two-sided *t*-test compared to 0; Object: 0.25± 0.028, $N = 99$, $P = 2.1 \times 10^{-14}$; Empty: 0.24 ± 0.023, $N = 130$, $P = 2.1 \times 10^{-19}$). There was no significant difference among the 3 conditions (*One-way ANOVA*: $F_{(1,428)} = 0.32$, $P = 0.73$). The result indicates that the high (or low) rate of an ACC selective cell during the delay period in a trial was accompanied with its high (or low) rate during the water consumption of the same trial.

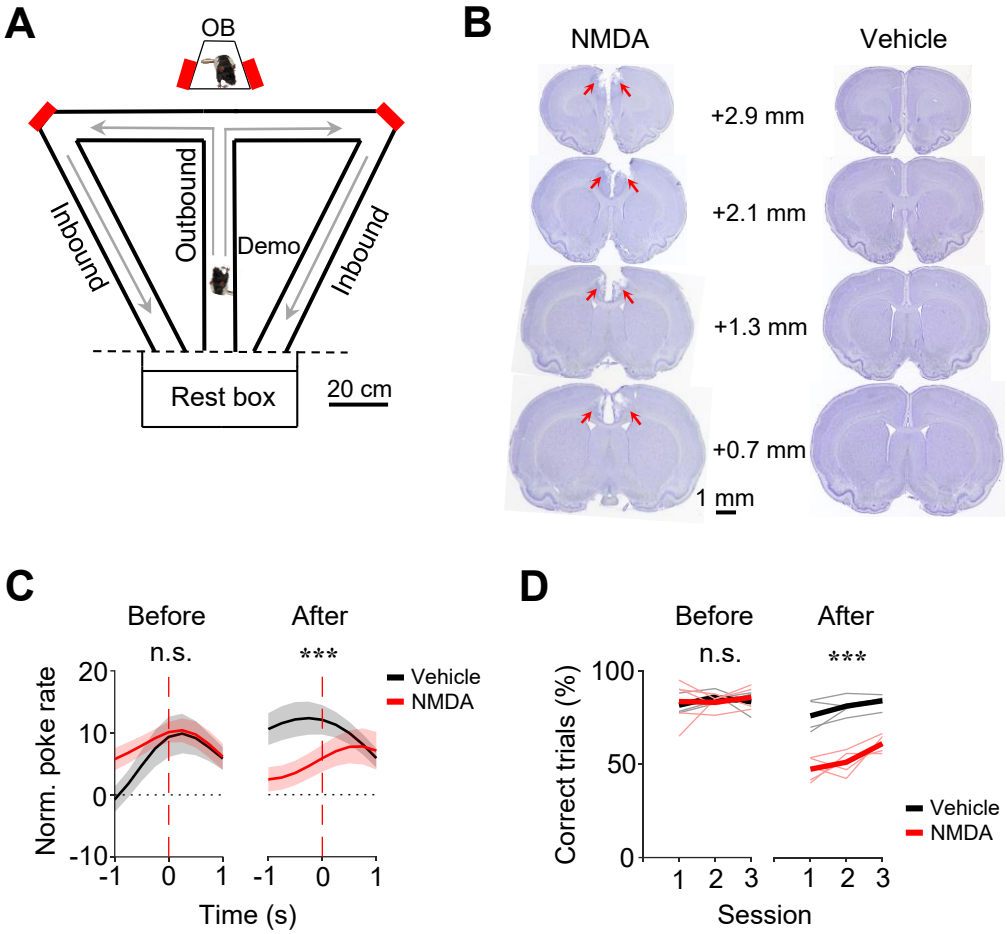

Figure 1. Performances of OBs in the observation box and in the maze depended on ACC.

(**A**) Behavioral apparatus consisting of an observation box (top), a continuous T-maze and a rest box (bottom). Red: reward site (water port); arrow: running direction. OB/Demo: observer/demonstrator rat.

(**B**) Coronal brain sections with NMDA and vehicle infusion. Arrow: lesion in ACC. Number: anteroposterior coordinate from the Bregma.

(**C**) Average (mean ± SEM) poke performance curves of OBs in the box for the 3 sessions before (Before) and the first 3 testing sessions 2 weeks after NMDA or vehicle infusion (After).

(**D**) Maze performances of OBs in each of Before and After sessions. Thin/thick line: individual rat/average performance.

***: $P < 0.001$, **: $P < 0.01$, *: $P < 0.05$, n.s.: not significant (same for all figures).

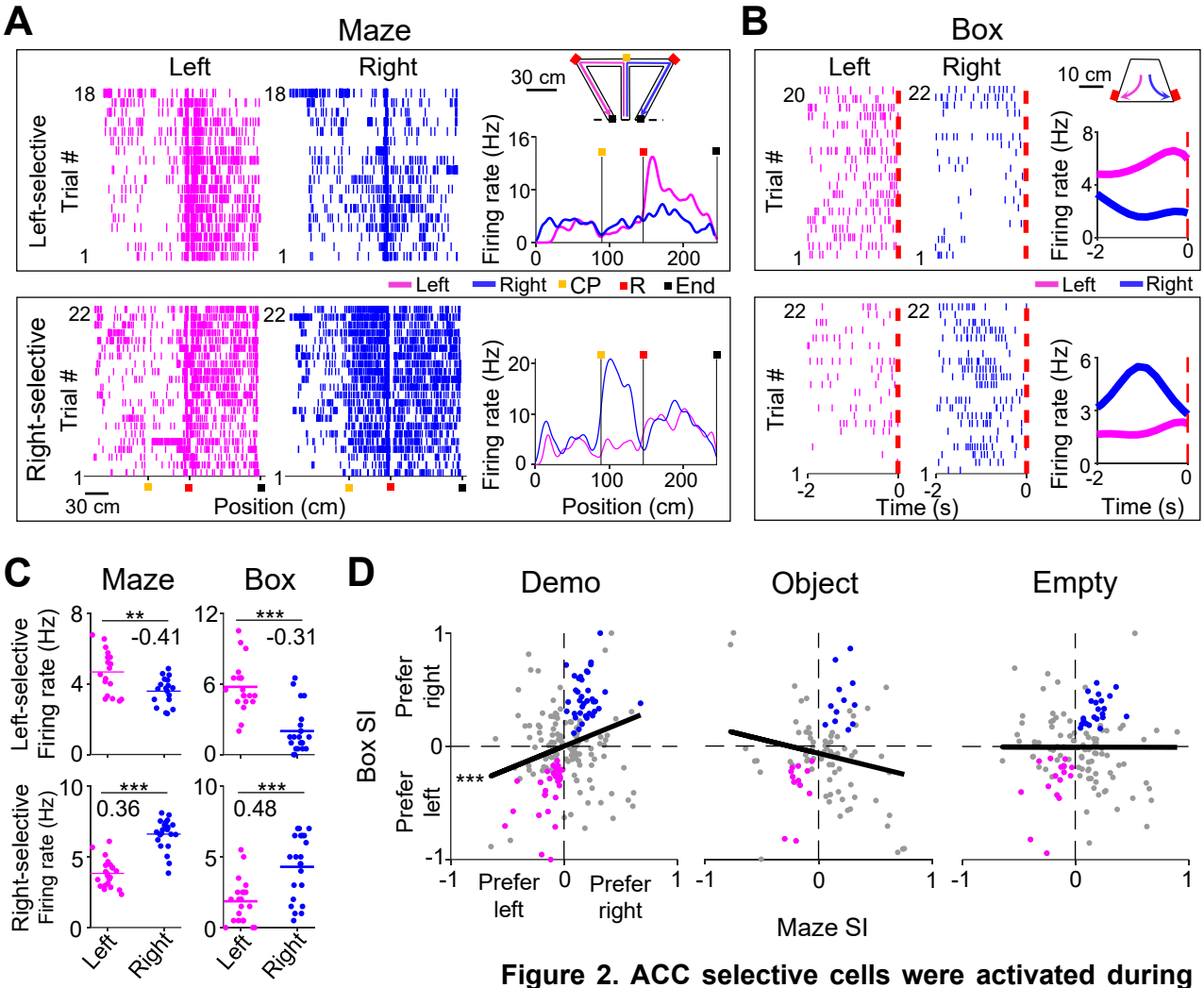

Figure 2. ACC selective cells were activated during delay periods in the observation box.

(**A**) Spike raster of an ACC left- (top) and an ACC right-selective (bottom) cell on the left (magenta) and right (blue) sides of the T-maze, and their average firing rates along the (linearized) trajectories on the two sides (right curves). Each tick is a spike. Each row is a trial. Color markers show maze landmarks: choice point (CP), reward site (R), end of side-arm (End). The two cells were from two different sessions. Error trials (top: 2 left and 4 right; bottom: 0) are excluded.

(**B**) Similar to (**A**), but for the same two cells during the delay period of each trial in the box: 2 s before the first rewarded poke (dash line, time 0). Note the higher rate on the same side of each cell's selectivity.

(**C**) Firing rates of the same two cells in (**A**-**B**) during each trial on the left/right side of the maze and during each delay period on the left/right side of the box. Note the similar selection indices (SIs, numbers) in the maze and in the box.

(**D**) SIs in the maze and in the box for all ACC selective cells under Demo, Object and Empty. Each dot is a cell. Black line: linear regression between maze and box SIs. Colored dots: cells with significant same-side selectivity in the box on the left (magenta) or right (blue).

(**E**) Percentages of ACC cells with significant same-side selectivity in the box (left/right combined, red lines) under Demo, Object and Empty, compared to random distributions (black) obtained by shuffling each cell's firing rates among all delay periods of left/right trials.

See also Figure S1, S2.

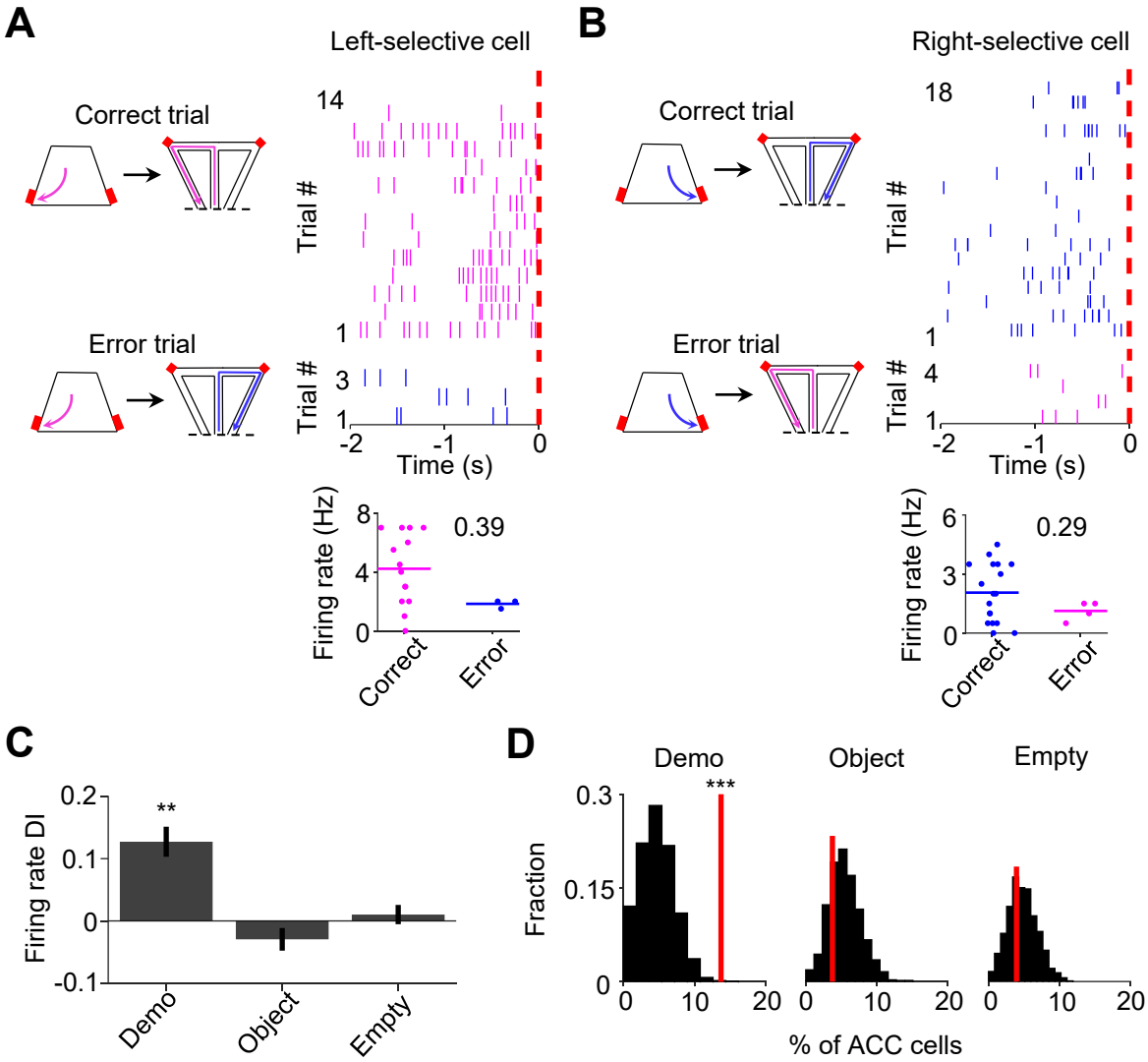

Figure 3. ACC cells with same-side selectivity in the box were less activated during delay periods of error trials.

(**A**) Left: illustration of a correct and an error trial when the Demo chose left in the maze. A trial was considered an error if the OB chose the opposite (right) side in the maze, after getting rewarded (on the left side) in the box. Red: reward sites. Right: trial-by-trial spike raster (top) of an ACC left-selective cell (in both the maze and box) and firing rates of this ACC cell in each correct/error trial (bottom) during delay periods of an example session. Each tick represents a spike. Magenta/blue: spikes in correct/error trials. Red dash line: OB's poke time (time 0). Number: firing rate difference index (DI) between correct and error trials for this cell.

(**B**) Similar to (**A**), but for an ACC right-selective cell when the Demo chose right in the maze. Blue/magenta: correct/error trials.

(**C**) Comparison of ACC cell DIs described in (**A**-**B**) during delay periods on their preferred side under Demo, Object and Empty.

(**D**) Percentages of ACC cells with same-side selectivity in the box that had significantly higher firing rate during delay periods of correct trials on their preferred side (left-selective and right-selective cells combined, red lines) under Demo, Object and Empty, compared to their shuffle-generated distributions (black).

See also Figure S3.

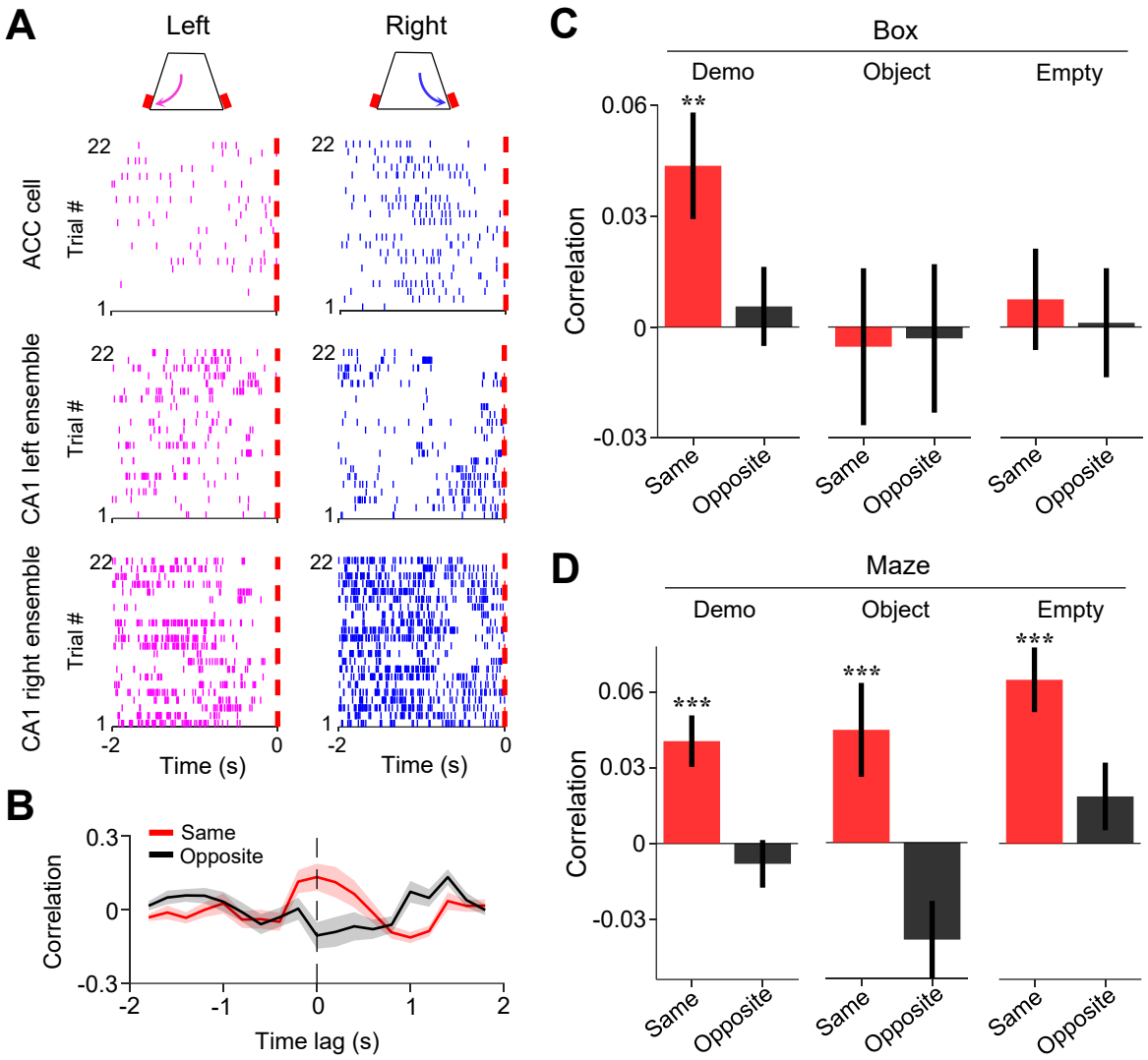

Figure 4. Activities of ACC cells were correlated with those of CA1 same-side ensembles during delay periods in the box.

(**A**) Trial-by-trial spike raster of an example ACC right-selective cell and its associated CA1 left and right ensembles during delay periods of left (magenta) and right (blue) trials of a session. Each tick is a spike. Red dash line: time of first rewarded poke in the box (time 0).

(**B**) Firing rate cross-correlation between the example ACC cell and its associated CA1 ensemble in (**A**). Red/black curves: average values over all trials in the session. Shaded areas: SEM. Note the peak correlation around time lag 0 (dash line) between the ACC cell and the same-side CA1 ensemble.

(**C**) Average correlations (mean ± SEM, at time lag 0) during delay periods between ACC cells and the CA1 same- (red) and opposite-side (black) ensembles under Demo, Object and Empty. Note the significant same-side correlation under Demo, but not under Object or Empty.

(**D**) Similar to (**C**), but for correlations during running laps in the maze. Note the significant same-side correlation under all three conditions, as expected.

See also Figure S4.

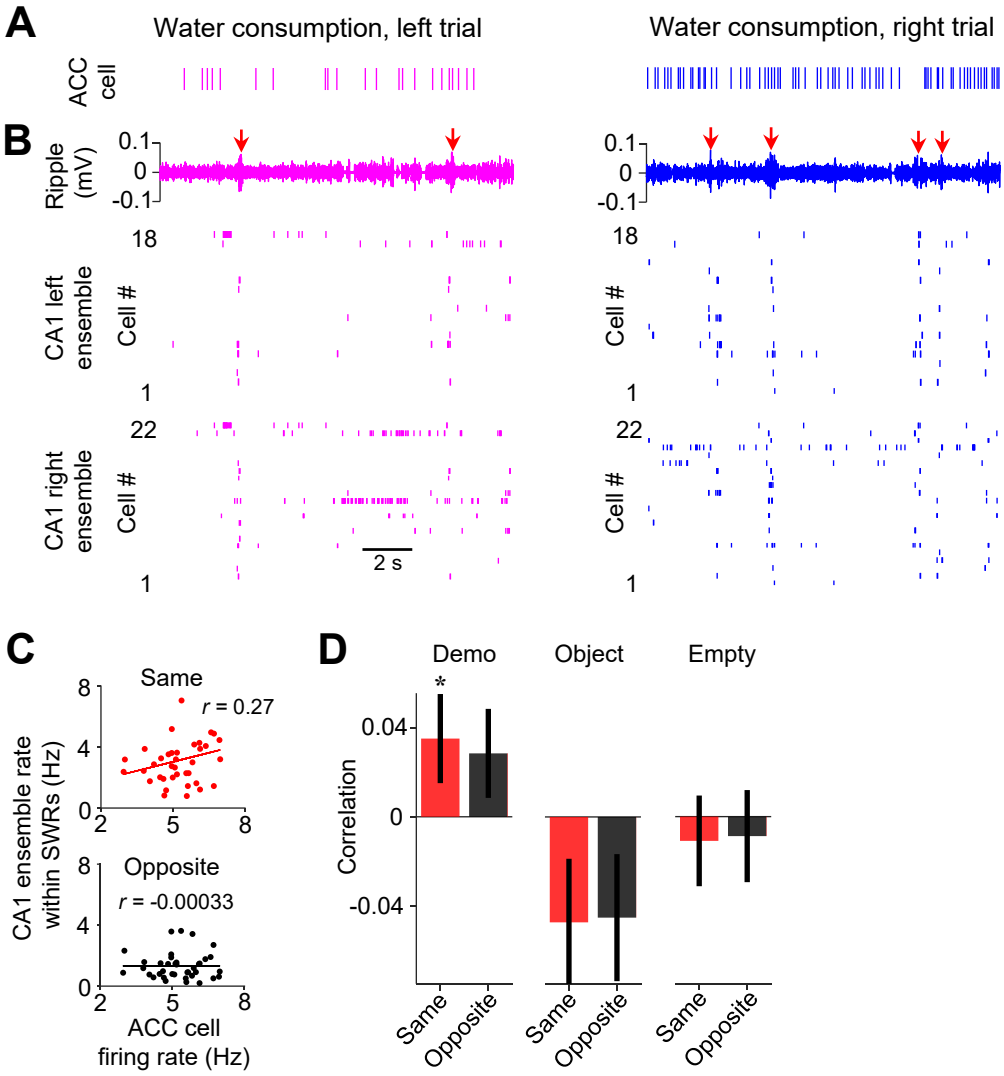

Figure 5. Activities of ACC cells were correlated with those of CA1 same-side ensembles during water consumption in the box.

(**A**) Spike raster of an example ACC right-selective cell during water consumption in the box for a left and a right trial of a session. Each tick is a spike.

(**B**) CA1 LFPs filtered within the ripple band (top) and spike raster of CA1 cells in the left (middle) and right ensemble (bottom) during the same time periods in (**A**). Arrows: SWRs. Note the population bursts associated with SWRs.

(**C**) Correlation (*r*) between trial-by-trial firing rates of the example ACC cell and its CA1 same- and opposite-side ensemble within SWRs during water consumption in the session. Each dot is a trial.

(**D**) Average correlations (mean ± SEM) for all ACC selective cells and their CA1 same- and opposite-side ensembles, as computed in (**C**), under Demo, Object and Empty.

See also Figure S5.

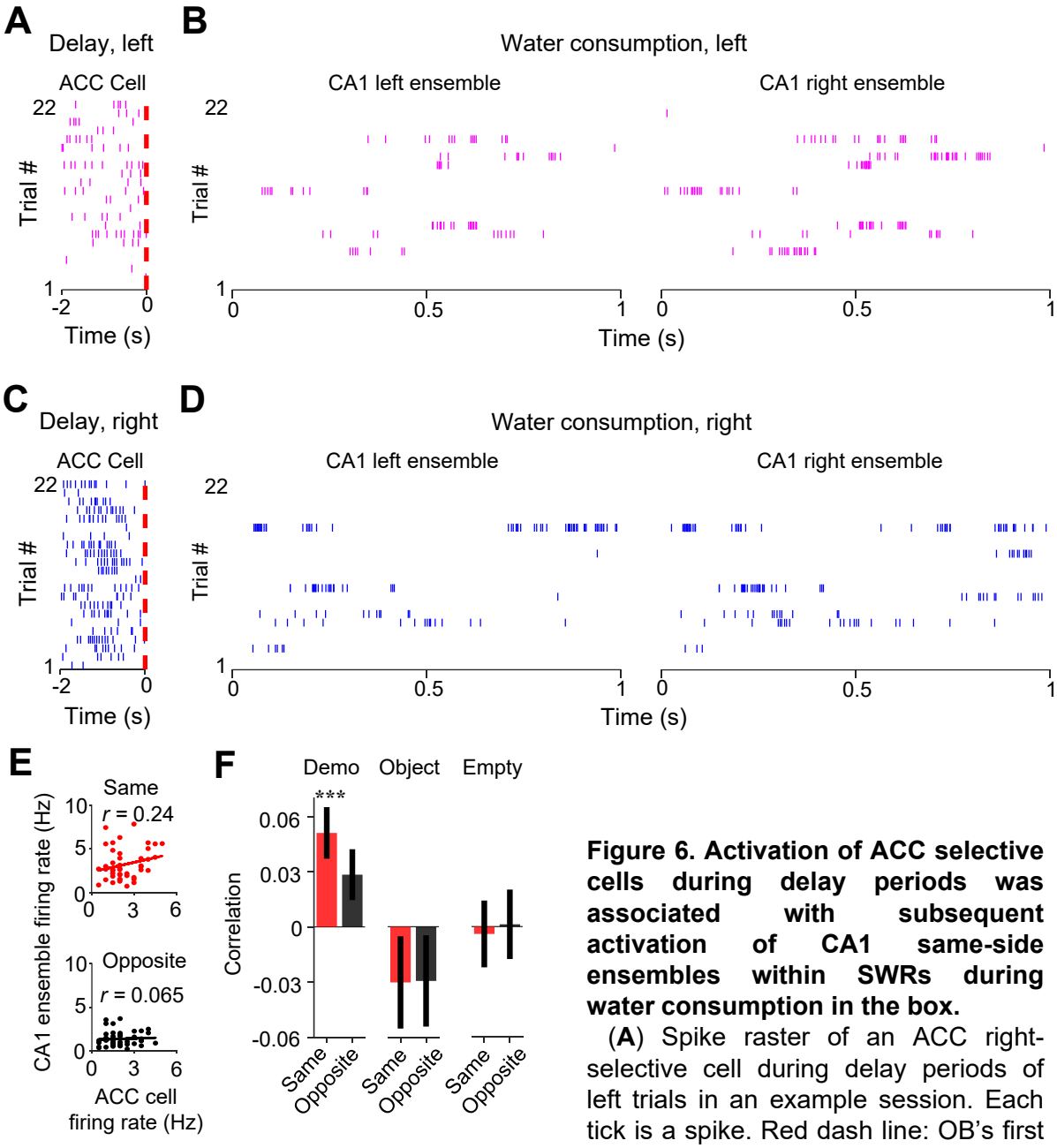

Figure 6. Activation of ACC selective cells during delay periods was associated with subsequent activation of CA1 same-side ensembles within SWRs during water consumption in the box.

(**A**) Spike raster of an ACC right-selective cell during delay periods of left trials in an example session. Each tick is a spike. Red dash line: OB's first rewarded poke in the box (time 0).

(**B**) Spike raster of CA1 left and right ensembles within SWRs during water consumption periods of the same (left) trials in (**A**). Only spikes within SWRs of a 1 s window are shown for clarity.

(**C**-**D**) Similar to (**A**-**B**), but for the same ACC (right-selective) during delay periods and same CA1 ensembles during water consumption periods in the right trials of the same session.

(**E**) Correlation (*r*) between trial-by-trial firing rates of the ACC cell during delay periods and its CA1 same- or opposite-side ensembles within SWRs during water consumption in the session. Each dot represents a trial.

(**F**) Average correlations (mean ± SEM) for all ACC selective cells and their CA1 same- and opposite-side ensembles, as computed in (**E**), under Demo, Object and Empty.

See also Figure S6.

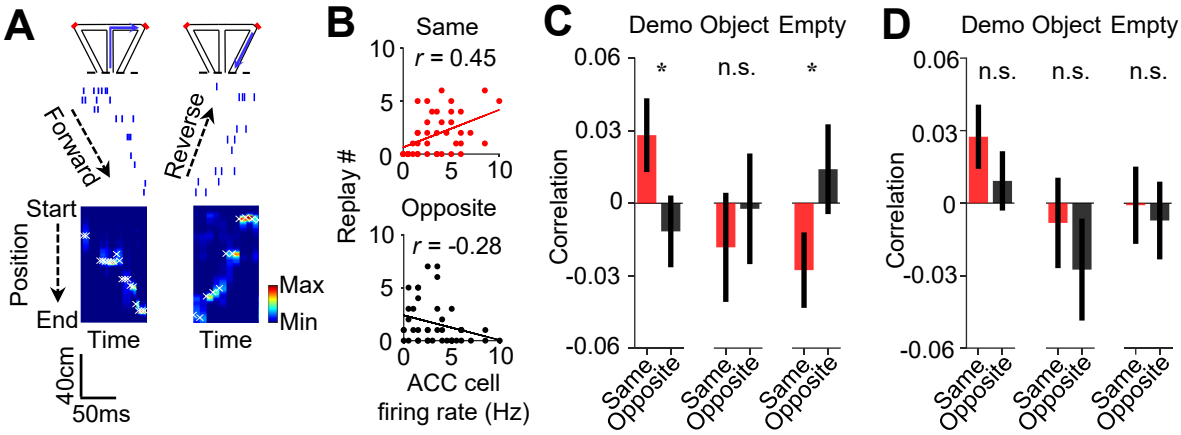

Figure 7. Activation of ACC selective cells during delay periods was associated with the replay of CA1 same-side ensembles during water consumption in the box.

(**A**) Spike raster (middle) of an example forward/reverse replay of the CA1 template cells corresponding to the right outbound/inbound trajectory (top). The Bayesian-decoded probability of trajectory positions at each time bin is shown at the bottom. x: decoded (peak probability) positions. Dashed line: replay order of spikes.

(**B**) Trial-by-trial correlation (*r*) between an example ACC cell's firing rate during delay periods and the number of replays for CA1 templates on the same- or opposite-side inbound trajectories of the ACC cell's selectivity. Each dot represents one trial.

(**C**) Average correlation values (mean ± SEM) for all ACC selective cells and the corresponding replay numbers for same- or opposite-side templates, as computed in (**B**), under Demo, Object and Empty. Note the higher same-side correlation under Demo, but not under Object or Empty.

(**D**) Similar to (**C**), but for outbound trajectories.

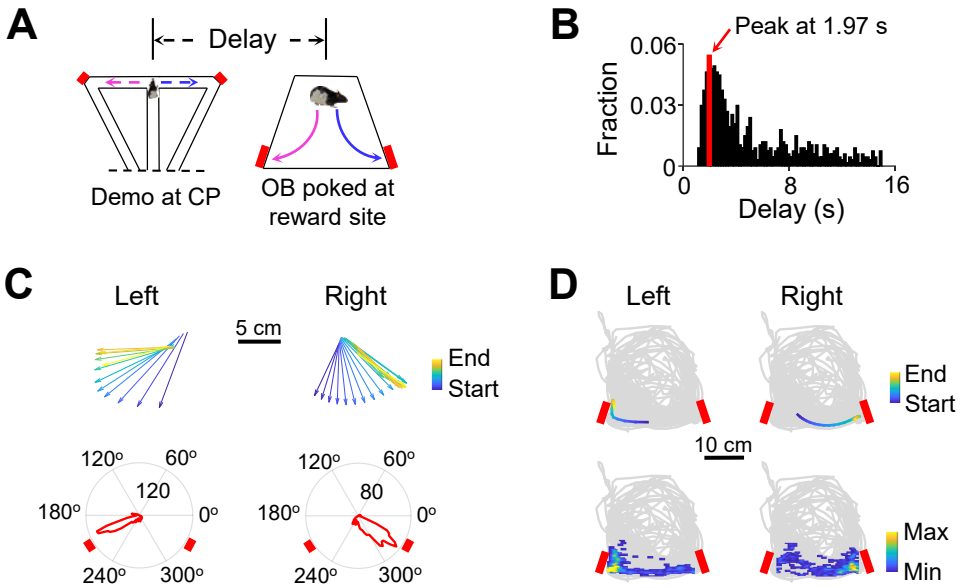

Figure S1. Behavior of OBs during delay periods in the observation box, related to Figure 2.

(**A**) Illustration of the delay time window of a trial: time interval between the Demo passing the T-maze choice point (CP) on a left (magenta) or right (blue) trajectory and the OB's first poke with reward at the corresponding water port in the box (not drawn proportionally).

(**B**) Distribution of the delay window duration for all trials of all recorded OBs under the Demo condition. Note the peak at 1.97 s.

(**C**) Top: an example OB's head direction within the 2 s (Start) delay period before first rewarded poke (End) in the box for a left and right trial. Head direction was computed in every 0.1 s time bin. Downward arrow shows the direction (270°) facing the T-maze.

Bottom: distribution of the OB's head direction in the 2 s delay periods of all trials in a session with left/right rewarded pokes. Number inside circle: radius length (count of time bins). Red rectangles: reward sites (at ~210°, 330°).

(**D**) Similar to (**C**), but for the OB's head position in the same left and right trial (top) and head position density during delay periods of all trials in the session. Bottom color bar: count of time bins. Gray trace: all head positions in the session.

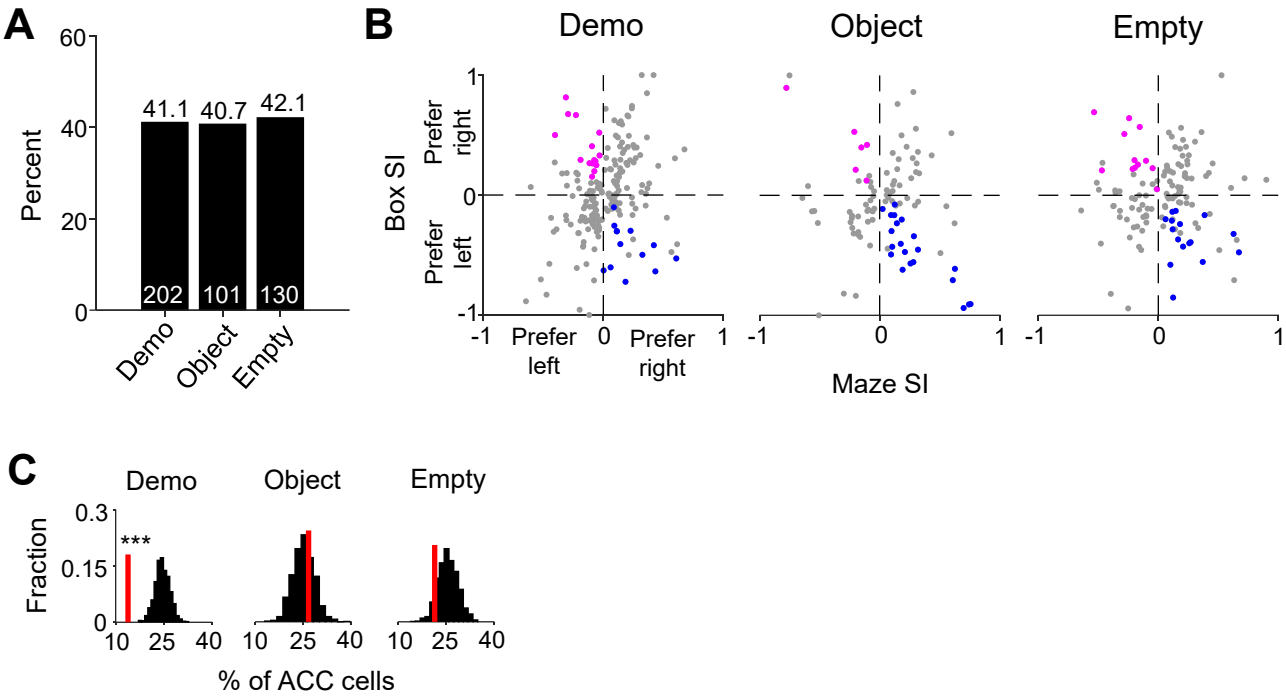

Figure S2. ACC cells with opposite-side selectivity in the box were fewer than the chance level under Demo, related to Figure 2.

(**A**) Numbers of ACC selective cells (white) and corresponding percentages among all recorded ACC cells under Demo, Object and Empty.

(**B**) SIs in the maze and in the box for all ACC selective cells under Demo, Object, and Empty. The plots are the same as in **Figure 2D**, but now the colored dots highlight those left- (magenta) or right- (blue) selective cells in the maze that had significant opposite-side selectivity in the box.

(**C**) Percentages of ACC selective cells with significant opposite-side selectivity in the box (red lines) under Demo, Object and Empty, compared to their random distributions (black) obtained by shuffling each cell's firing rates among all delay periods of left and right trials in the box. Demo: 14%, Z = -4.1, P = 2.1 x 10^{-5}, Z-test; Object: 27%, Z = 0.47, P = 0.32; Empty: 22%, Z = -1.2, P = 0.89.

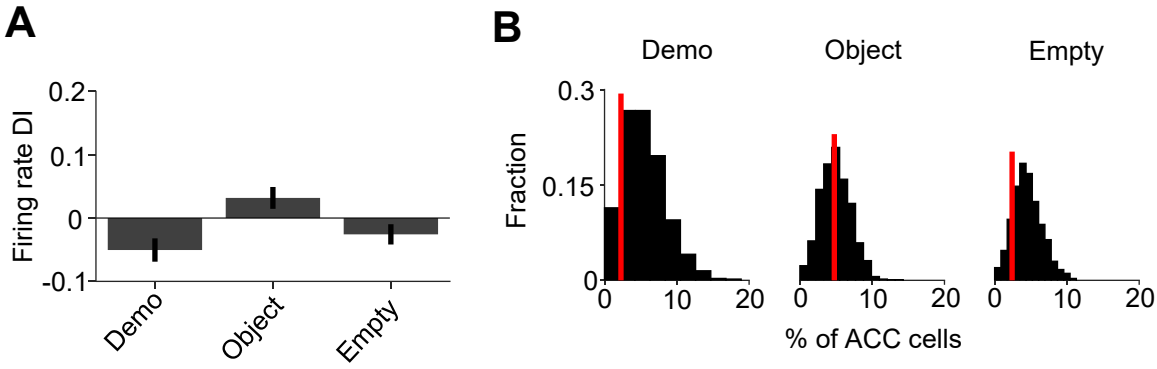

Figure S3. ACC cells with same-side selectivity in the box did not differ in firing rate during delay periods between correct and error trials on their non-preferred side, related to Figure 3.

(**A**) Average DIs (mean ± SEM) of ACC cells with same-side selectivity in the box on their non-selective side between delay periods of correct and error trials under Demo, Object and Empty. The DIs were not significantly different from 0 (Demo: -0.051 ± 0.030, N = 44, P = 0.11, two-sided t-test; Object: 0.032 ± 0.021, N = 84, P = 0.13; Empty: -0.026 ± 0.016, N = 124, P = 0.11). There was a significant difference among the 3 conditions (*One-way ANOVA*: $F_{(1,251)} = 3.54$, $P = 0.030$).

(**B**) Percentages of ACC cells with same-side selectivity in the box that had significantly higher rate during delay periods in correct trials on their non-preferred side (red, left-selective and right-selective cells combined) under Demo, Object and Empty, compared to shuffle-generated distributions (black). The percentage was not significant from the chance level under Demo (2.3%, Z = -0.77, P = 0.78, Z-test), Object (4.8%, Z = -0.0062, P = 0.50) or Empty (2.4%, Z = -1.2, P = 0.88).

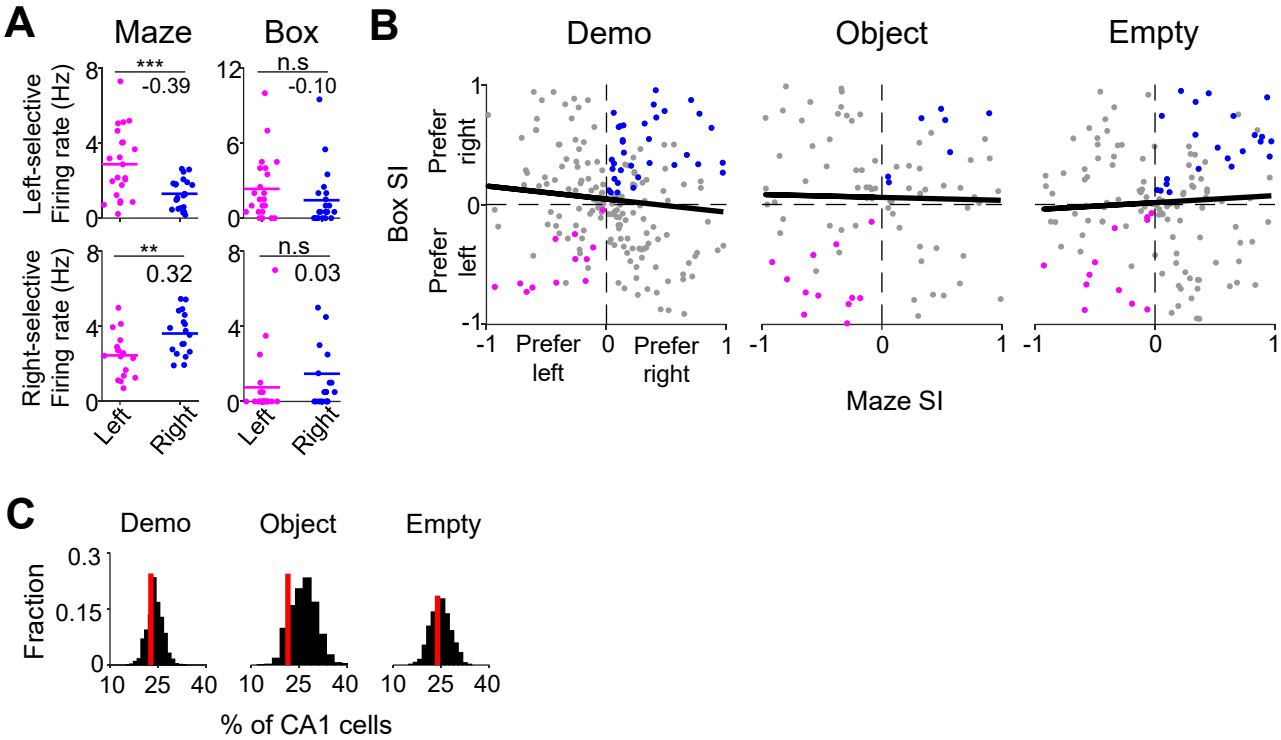

Figure S4. CA1 cells with same-side selectivity in the box were not significantly different from the chance level, related to Figure 4.

(**A**) Firing rates of two example CA1 cells during running in each trial on the left/right side of the maze and during each delay period in the box. Note different SIs (numbers) between the maze and box. (Left-selective cell: Maze: P = 3.3 x 10^{-4}, two-sided t-test; Box: P = 0.11; Right-selective cell: Maze: P = 0.0022; Box: P = 0.15)

(**B**) SIs in the maze and in the box for all CA1 cells active in the maze under Demo, Object and Empty. Colored dots: cells with significant same-side selectivity in the box on the left (magenta) or right (blue). Black line: linear regression between the maze and box SIs. There was no significant correlation under any of the conditions (Demo: R = -0.10, P = 0.93, *Pearson's r*; Object: R = -0.025, P = 0.59; Empty: R = 0.061, P = 0.24).

(**C**) Percentages of CA1 cells with significant same-side selectivity in the box (left/right combined, red lines) under Demo, Object and Empty, compared to their distributions (black) obtained by random shuffling of each cell's firing rates among all delay periods of left/right trials. The actual percentage was not significantly different from the random distribution under any of the conditions (Demo: 23%, Z = -0.54, P = 0.70, Z-test; Object: 22%, Z = -1.3, P = 0.91; Empty: 24%, Z = -0.38, P = 0.65).

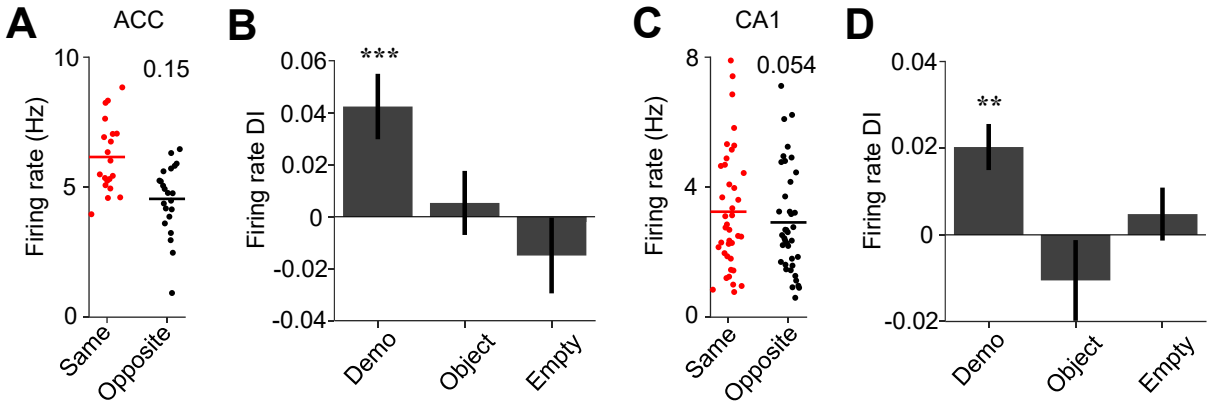

Figure S5. Activities of ACC selective cells and CA1 ensembles during water consumption in the box differed between same- and opposite-side of their selectivity, related to Figure 5.

(A) Trial-by-trial firing rates of a left-selective ACC cell during water consumption in the box on the same- and opposite-side of its selectivity in an example session. Each dot is a trial. Horizontal lines: mean values. Number: firing rate difference index (DI) between same- and opposite-side for this ACC cell.

(B) Average firing rate DIs over all ACC selective cells during water consumption under Demo, Object and Empty. The DIs were significantly higher than 0 under Demo (0.042 ± 0.013, N = 200, P = 9.1 x 10^{-4}, two-sided t-test), but not under Object (0.0053 ± 0.018, N = 99, P = 0.76) or Empty (-0.015 ± 0.018, N = 130, P = 0.41). There was a significant difference among the 3 conditions (*One-way ANOVA* test: $F_{(1,427)}$ = 4.0, P = 0.019).

(C-D) Similar to (**A-B**), but for firing rates of CA1 ensembles on the same- and opposite-side of ensembles. The average DIs in (**D**) were significantly higher than 0 under Demo (0.020 ± 0.0053, N = 19, P = 1.3 x 10^{-3}, , two-sided t-test), but not under Object (-0.011 ± 0.012, N = 11, P = 0.41) or Empty (0.0048 ± 0.0074, N = 13, P = 0.53). There was a significant difference among the 3 conditions (*One-way ANOVA* test: $F_{(1,42)}$ = 3.9, P = 0.028).

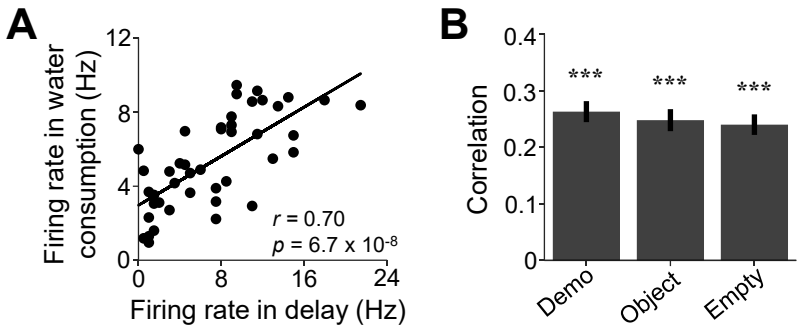

Figure S6. Activities of ACC selective cells during delay periods were correlated with their activities during water consumption periods in the box, related to Figure 6.

(**A**) Trial-by-trial correlation (*r*) between the firing rates of an example ACC cell during delay periods and during water consumption in all trials of a session. Each dot represents a trial.

(**B**) Average correlation values (mean ± SEM) for all ACC selective cells under Demo, Object and Empty. The correlations were significant under all the 3 conditions (Demo: 0.26 ± 0.019, N = 200, P = 5.7 x 10^{-32}, two-sided *t*-test compared to 0; Object: 0.25± 0.028, N = 99, P = 2.1 x 10^{-14}; Empty: 0.24 ± 0.023, N = 130, P = 2.1 x 10^{-19}). There was no significant difference among the 3 conditions (*One-way ANOVA*: $F_{(1,428)}$ = 0.32, P = 0.73). The result indicates that the high (or low) rate of an ACC selective cell during the delay period in a trial was accompanied with its high (or low) rate during the water consumption of the same trial.